JOURNAL OF GEOPHYSICAL RESEARCH, VOL. 101, NO. D5, PAGES 9489–9508, APRIL 27, 1996

Noctilucent clouds and the thermal structure near the Arctic mesopause in summer

F.-J. Lübken, K.-H. Fricke, and M. Langer

Physikalisches Institut der Universität Bonn, Bonn, Germany

Abstract. In the summers of 1993 and 1994 a series of meteorological rockets and sounding rockets were launched from the Andøya Rocket Range (69°N) during the SCALE and ECHO campaigns in order to investigate the state of the mesosphere and lower thermosphere (SCALE = "SCAttering Layer Experiment"; ECHO indicates that radar and lidar echoes are investigated). At the same location a Rayleigh lidar was operational during these campaigns and searched for enhanced backscatter signals from the upper mesosphere indicative of the presence of noctilucent clouds (NLC). In five cases the lidar detected a NLC and the atmospheric temperature profile was obtained simultaneously by in situ techniques. A literature survey shows that there are only three more cases of unambiguous and simultaneous observations of NLC temperature and altitude. The temperature profiles obtained during SCALE and ECHO are as expected for the high-latitude summer season: The mean mesopause temperature is 135 K at an altitude of 87.5 km. The variability of the temperatures is smaller above ~84 km altitude than below. The mean temperature below the mesopause shows a remarkable repeatability ever since the first measurements 30 years ago; at the lower edge of the NLC heights (82 km) it is again and again observed to be in the range 150 ± 2 K and the variability within each data set is only a few Kelvins. Such an "equithermal submesopause" in summer puts a serious constraint on any model prediction of secular changes of temperatures in the upper mesosphere. The mean altitude of the NLCs as determined from our lidar measurements is 83.1 km which is surprisingly close to the very first height determinations more than 100 years ago. It is conceivable that this repeatability in altitude reflects a similar repeatability of the thermal structure. There is no apparent correlation between the conditions at the mesopause and the occurrence of NLCs at lower altitudes. The physical reason behind this is presumably related to the fact that the wind direction changes at ~87 km height, which implies that the air masses observed above the rocket site near mesopause altitudes have been advected from different locations than those at NLC heights. The NLCs are always located below the mesopause, and the temperature in the NLC layer is observed to be lower than 154 K. Our results are compatible with the idea that NLCs consist of ice particles which start to nucleate around the mesopause, sediment to lower altitudes while growing, become observable by the lidar and/or by the naked eye, and finally evaporate once they approach the higher temperatures around 82 km.

1. Introduction

Noctilucent clouds (NLC) are an optical phenomenon in the upper summer mesosphere at high latitudes that has stimulated many scientific investigations since they were first reported in the scientific literature more than 100 years ago. Excellent reviews of our actual knowledge concerning observational statistics of these clouds and the physical conditions at the height where they are observed are available in the literature [*Fogle and Haurwitz*, 1966; *Turco et al.*, 1982; *Gadsden and Schröder*, 1989; *Thomas*, 1991; *Avaste*, 1993]. After the first observations it was realized quickly from the spectrometric analysis of the scattered light and from geometric considerations that the light observed at the ground is actually sunlight scattered at particles from around the mesopause. Model simulations have supported the now commonly accepted view that these particles mainly consist of ice. The formation of these ice particles is initiated by water vapor condensing on preexisting nuclei (i.e., dust or large ions) around the mesopause. Then the particles grow and sediment to lower altitudes, where they finally evaporate when they

Paper number 96JD00444.
0148-0227/96/96JD-00444$05.00

encounter increasing temperatures [*Reid*, 1975; *Jensen and Thomas*, 1988; *Garcia*, 1989]. These particles are presumably also the constituents of the scattering clouds being observed from satellites at approximately the same altitude during the summer season. These clouds have been given a different name ("polar mesospheric clouds", PMC), although they most likely have the same origin. Noctilucent clouds and polar mesospheric clouds have gained more and more importance in recent years, when it was realized that their increased occurrence rate observed in recent decades may be related to anthropogenically induced temperature and/or humidity changes in the upper atmosphere [*Gadsden*, 1990; *Thomas et al.*, 1989; *Thomas*, 1995]. The importance of NLCs in this context is based on the fact that they represent the longest record of observations available concerning possible trends in the middle atmosphere.

Despite the fact that the atmospheric temperature is the most sensitive parameter controlling the existence of NLC particles, there have been only very few simultaneous measurements of the altitude of NLCs and the thermal structure around the mesopause. These measurements were made by sounding rockets that were launched from within the polar circle when the NLC was reported from a ground-based or an airborne observer being located typically some hundred kilometers away from the rocket range in order to meet appropriate visual conditions for observations. This situation changed a few years ago, when it was demonstrated that lidars are capable of detecting NLCs at latitudes within the polar circle (e.g., directly above the rocket range), where visual observations are impossible due to the permanently bright sky [*Hansen et al.*, 1989; *Thayer et al.*, 1995; *Langer et al.*, 1995a]. These lidars detect the presence of aerosols in the upper mesosphere as an enhanced backscatter relative to the signal expected from a clean molecular atmosphere. We deliberately call these signal intensifications "noctilucent clouds" since they occur at the same latitude, same altitude, and same time of the year as the optical phenomenon known under this name. Furthermore, both observations result from the same physical process, namely, the enhanced scatter of visual light from aerosol particles. These lidars not only give the exact altitude of the NLC layer, but also allow one to study the variability of the cloud due to horizontal structures or to temporal evolutions (in fact, both phenomena are not distinguishable by the lidar observations). On the other hand, lidar measurements of atmospheric densities and temperatures are systematically hampered during summer by the relatively high noise level during daylight measurements. In addition, NLC particles themselves increase the amount of scattered light to an unknown extent. It is therefore important to measure the temperature profile (or alternatively, the neutral air density profile) by a method which is not influenced by the presence of NLCs, for example, by meteorological rockets.

In the summers of 1993 and 1994, coordinated measurements by ground-based and in situ techniques were performed at Andøya (69°N) during the SCALE and ECHO campaigns, respectively. It is the main purpose of this paper to report about lidar measurements of the altitude of the noctilucent clouds and simultaneous observations of the thermal structure of the mesosphere above the lidar location by means of meteorological rockets ("falling spheres"). We will also refer to some recent temperature measurements by falling spheres in May 1995, which were performed from the Andøya Rocket Range in the scope of the AEROSOL 2 campaign.

In the next section we will introduce the experimental techniques relevant for our observations. New results obtained during SCALE, ECHO, and AEROSOL 2 are presented in section 3. We will then give an overview of the data available in the literature concerning simultaneous observations of NLC altitudes and temperatures in section 4. Finally, we will discuss the impact of the data on our understanding of NLCs and their atmospheric environment in section 5.

2. Method of Observations

2.1. The Rayleigh Lidar

Since the end of 1990, a Rayleigh lidar has been operational at the Andøya Rocket Range on a campaign basis. This lidar is capable of measuring during daylight with a reasonably short integration time of a few minutes (for technical details, see *Langer et al.* [1995a]).

From the observed lidar signal we derive the backscatter ratio R, which is defined as

$$R = \frac{\text{total signal}}{\text{molecular signal}} = 1 + \frac{\beta_A}{\beta_M}, \qquad (1)$$

where β denotes the backscatter coefficient and the subscripts A and M refer to aerosols and molecules, respectively. The presence of aerosols in the atmosphere results in an enhanced backscattered signal (relative to the scatter from molecules) and leads to backscatter ratios larger than unity. The required molecular signal at the altitude of the mesopause aerosol layer is obtained from the falling sphere density profile or from interpolation of the lidar signal across the width of the layer if no density measurements are available.

Since mid-1994, a second Rayleigh lidar has been installed within the Arctic Lidar Observatory for Middle Atmosphere Research (ALOMAR), just 2 km line-of-sight distance from the Bonn University lidar [*von Zahn et al.*, 1995]. A comparison of both lidar observations has shown very good agreement [Nussbaumer et al., First simultaneous and common-volume observations of NLC and PMSE by lidar and radar, submitted to *Journal of Geophysical Research*, 1996] (hereafter refered to as submitted manuscript, 1996).

2.2. Falling Spheres and TOTAL/CONE Ionization Gauges

The passive falling sphere technique has been described in the literature [cf. *Jones and Peterson*, 1968; *Schmidlin*, 1991]. The sphere, made of metalized my-

lar, is typically released at 110 km altitude and inflated to 1-m diameter. It passively falls in the atmosphere, and its descent trajectory is tracked by a high-precision radar. From the radar position the first and second derivatives of the sphere trajectory with respect to time are obtained, which are then used in the equations of motion to determine atmospheric density and horizontal winds. Temperatures are obtained by integrating the density profile assuming hydrostatic equilibrium. The height dependent sphere reaction time constant introduces a smoothing of the density, temperature, and wind profiles. The smallest scales detectable are typically 8, 3, and 0.8 km at 85, 60, and 40 km, respectively. The uncertainty of the absolute temperature data obtained from the falling sphere is typically 7, 3, and 1.5 K at 90, 80, and 70 km altitude, respectively.

Absolute number densities with high spatial resolution (few meters) were measured in the altitude range from ~115 to 90 km with the combined neutral and electron (CONE) instrument on board the TURBO payload. Temperatures are derived from the density profile assuming hydrostatic equilibrium. CONE basically consists of an ionization gauge (for more details, see *Lübken* [1996]). The TURBO sounding rockets and the falling spheres launched during SCALE and ECHO are listed in Table 1.

In order to judge the accuracy of our falling sphere data, it is important to consider all sources of uncertainties and, if possible, compare this technique with other instruments. During the Dynamics Adapted Network for the Atmosphere campaign (DYANA) such a comparison was feasible since measurements of densities and temperatures were performed simultaneously by different techniques at the same location [*Offermann*, 1994]. It is important to note that these measurements were performed during night in winter. A summary of the comparison of Rayleigh lidar and falling sphere results is presented by *Lübken et al.* [1994]. It was found that the measurements of the various techniques are reliable and that, in general, the error bars given are realistic.

3. Simultaneous Measurements of NLC Altitude and Temperature

Before we start presenting the data measured during SCALE and ECHO, we note that there is a horizontal distance of typically 40 to 45 km at an altitude of 85 km between the atmospheric volumes probed by the lidar and by the falling sphere. This is due to the fact that the lidar is measuring vertically, whereas the falling sphere is launched such that the apogee of the rocket is approximately at a horizontal distance of 25 km away from the

Table 1. Overview of Falling Sphere and Lidar Measurements During the SCALE and ECHO Campaigns

Flight	Date	Time	Mesopause			Lidar		NLC?		
Label		UT	T_{min}	$z(T_{min})$	$S(T_{min})$	max z	Percentage of Time	z	T	R_{max}
			K	km		km		km	K	
SCALE Campaign in 1993										
SCS01	July 27	0015	136	88.4	1.8	73 km	100	no		
SCS02	July 28	2207								
SCT03	July 28	2223	135	88.0	2.8	55 km	100	82.6	151	239
SCS04	July 28	2238								
SCT06	Aug. 1	0146	129	84.8	40	50 km	20	(no)		
SCS07	Aug. 1	0206								
ECHO Campaign in 1994										
ECS01	July 28	2220	121	88.6	488	65 km	90	no		
ECT02	July 28	2239				65 km	70	no		
ECS03	July 28	2303	122	87.4	308	65 km	60	no		
ECS04	July 29	2156	142	83.8	0.9	68 km	100	no		
ECS06	July 31	0027	135	86.2	3.7		100	83.6	140	114
ECT07	July 31	0050				69 km				
ECS08	July 31	0109	136	89.2	0.1		80	82.3	150	115
ECS09	Aug. 02	2213	138	83.8	2.6	69 km	100	83.6	138	26
ECS11	Aug. 10	2348	125	88.2	71	78 km	60	no		
ECT12	Aug. 12	0053				60 km	100	no		
ECS13	Aug. 12	0114	135	86.4	3.6	60 km	60	no		
ECS14	Aug. 17	2112	119	89.8	498	85 km	100	no		
ECS15	Aug. 17	2255	137	89.4	0.93	85 km	100	82.1	147	47

The third letter of the flight label indicates the type of rocket flown; "S" is falling sphere and "T" is TURBO sounding rocket. At the mesopause we have listed the temperature, T_{min}, the altitude, $z(T_{min})$, and the degree of saturation, $S(T_{min})$, assuming a water vapor mixing ratio of 1 ppmv. The "max z" is the altitude at which the Rayleigh backscatter signal from atmospheric molecules approaches the noise limit. Percentage of time is that amount of time around the rocket launch (± 1h) when the sky was sufficiently clear. R_{max} is the maximum lidar backscatter ratio within the NLC layer. More details are explained in the text.

Table 2. Nights With Lidar Observations of Noctilucent Clouds (NLC) during SCALE and ECHO

Lidar NLC		
Date	Time UT	Falling Sphere
	SCALE 1993	
July 28–29	2120 – 2242	SCS02/04
Aug. 7–8	2000 – 0250	N/A
Aug. 9–10	2151 – 2207	N/A
	ECHO 1994	
July 30–31	2334 – 0125	ECS06/08
Aug. 2–3	2120 – 0200	ECS09
Aug. 8–9	1615 – 2125	N/A
Aug. 17–18	2220 – 2325	ECS14/15

The times indicate the first and last appearance of a NLC in that night. Occasionally, the clouds appeared only sporadically during that period. N/A is not available.

launcher, which is only 1 km from the lidar. We will discuss the impact of this distance on our comparison later. We should also note that the falling sphere wind measurements show that the mean wind speed is approximately 60 m/s at NLC altitudes and that the wind is blowing from the northeast (typical wind direction is ~60°). The wind is blowing almost perpendicular to a line connecting the volumes probed by the lidar and the falling sphere at NLC heights.

3.1. Lidar Observations During SCALE and ECHO

There are a total of 34 nights with lidar observations in the summers of 1993 and 1994, but only in 7 nights were NLCs detected by the lidar. These nights are listed in Table 2. First lidar results are presented by *Langer et al.* [1995a,b] and *Nussbaumer et al.* (submitted manuscript, 1996). In four of these seven nights, falling sphere temperature profiles are available.

As an example of the quality of the lidar data, we show in Figure 1 (left) the lidar counts and (right) the backscatter ratio measured during the night of August 17–18, 1994. Data were integrated in a time slot of 16 min centered around the falling sphere launch ECS15 at 2255 UT. There is undoubtedly an enhanced backscatter signal around 82 km, which we interpret as being due to the presence of aerosol particles. In this example the layer is very thin (only six range gates corresponding to 900 m), with very sharp gradients at the bottom and at the top. The maximum ratio of the observed to the expected molecular signal, which is the backscatter ratio defined in (1), is 22 at an altitude of 82.4 km. The layer altitude is known with an accuracy of ± 75 m, which is half the range gate of the lidar.

As an example of the evolution of a NLC layer as observed by lidar, we show in Figure 2 a contour plot of measurements during the night of July 30–31, 1994 (this particular example was chosen since two falling spheres were launched in this night). The lidar first detected a NLC at 2334 UT at an altitude of 83.3 km, and a strong and persistent NLC layer with backscatter ratios of up to 200 developed within a half hour. The NLC layer stayed constant in altitude until approximately 0020 UT, when it started to descend, and finally reached an altitude of 82.5 km at 0120, where it disappeared. Since the lidar sounds the atmosphere vertically, we cannot distinguish between a layer descending in altitude and a layer being tilted and drifting through our laser beam. We will come back to this point in section 5.4.

Two falling spheres were launched during the night of July 30–31, 1994, one at the time when the layer started

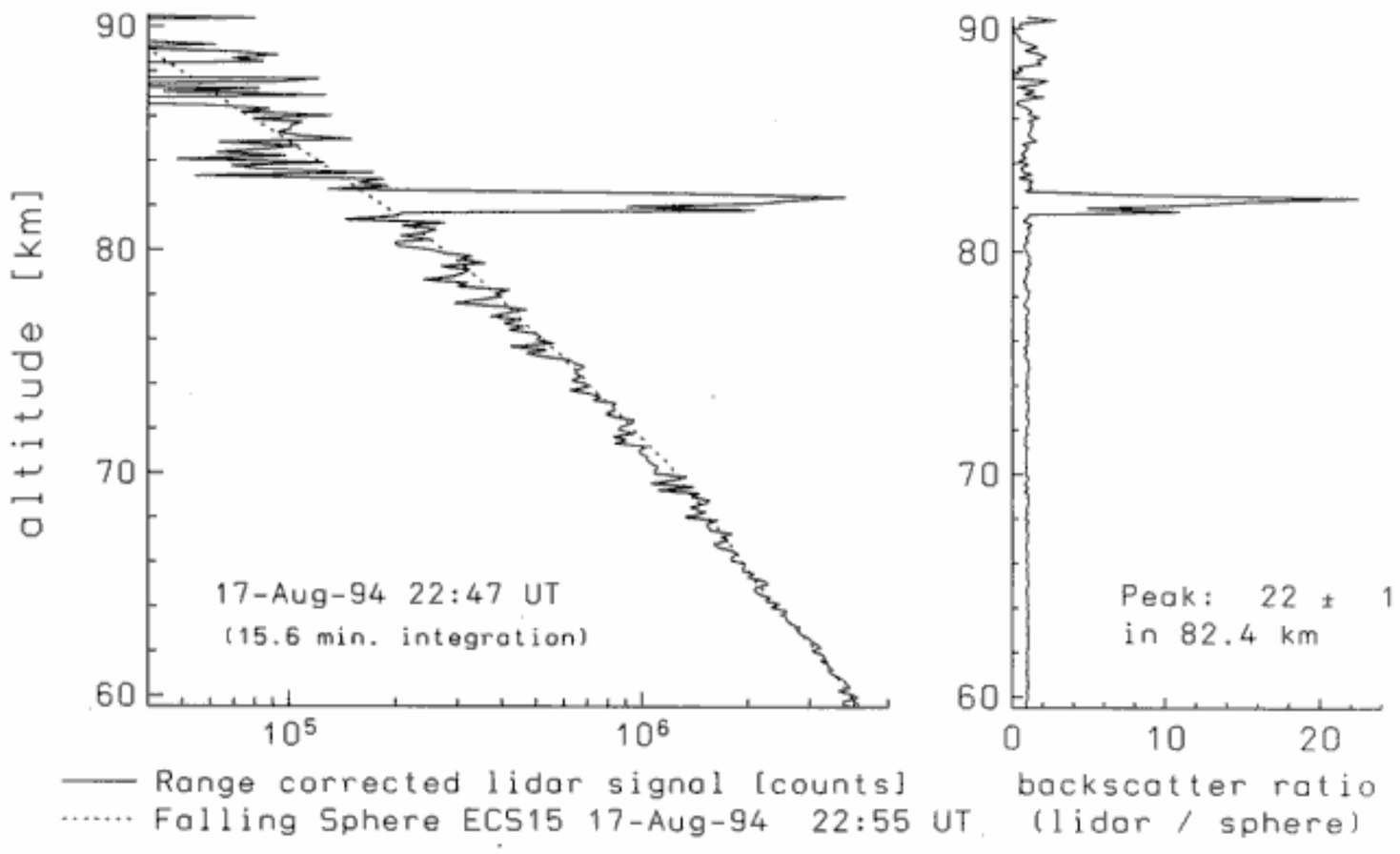

Figure 1. Rayleigh lidar signal (range corrected) and backscatter ratio as a function of altitude during the night of August 17–18, 1994. The profile was obtained in 15.6 min of integration time centered on the falling sphere flight ECS15. The drastic increase of the backscattered signal at approximately 82 km is due to aerosol particles deliberately called noctilucent clouds in this paper. The dashed line at left is the lidar equivalent molecular signal deduced from the densities measured by the falling sphere ECS15.

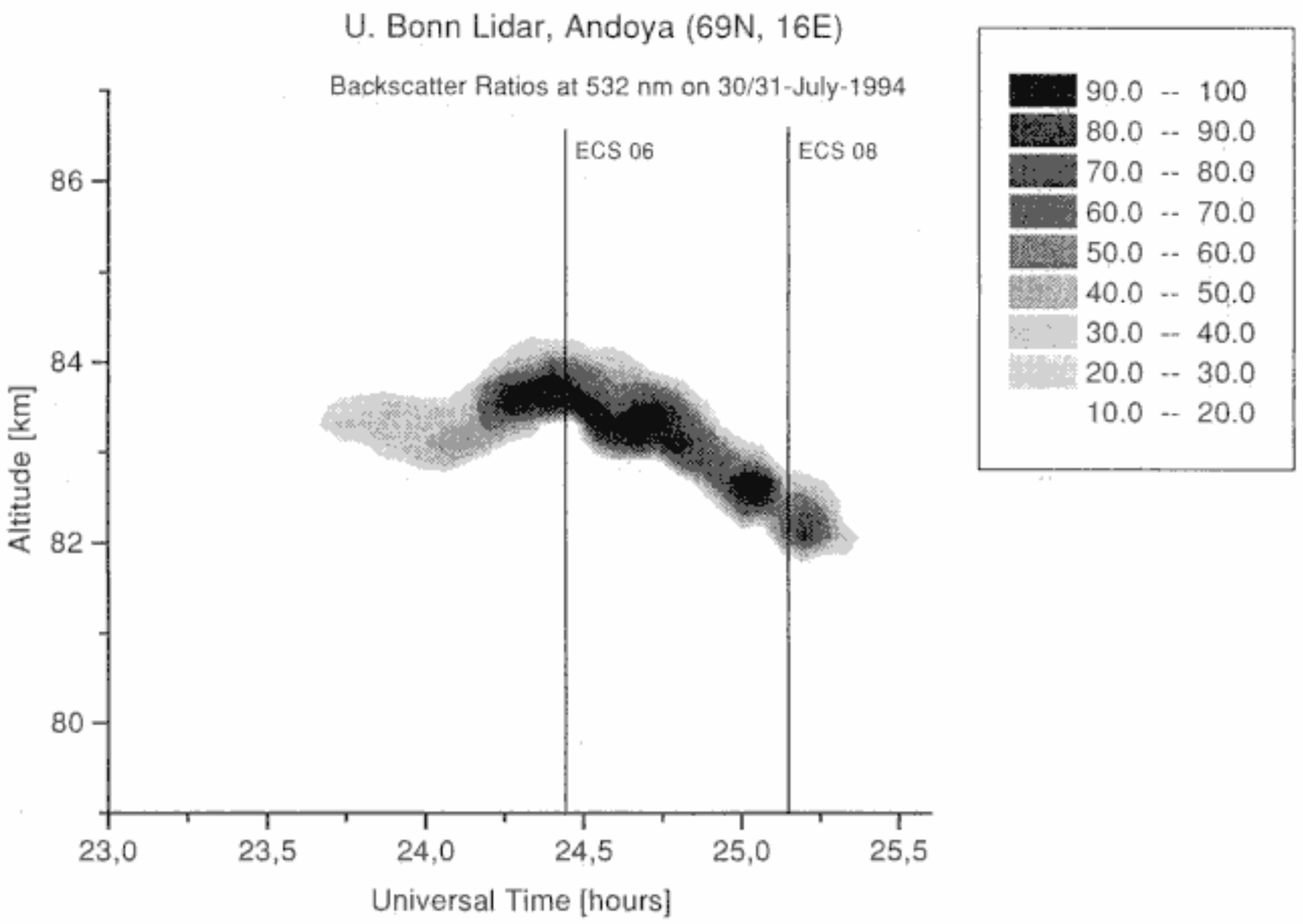

Figure 2. Contour plot of the backscatter ratio measured during the night July 30–31, 1994, in the scope of the ECHO campaign. The contour levels are explained in the inset. The two vertical lines indicate the falling sphere launches labeled ECS06 and ECS08, respectively.

to decrease in altitude (ECS06) and one shortly before the layer disappeared (ECS08). The times of launches are marked by vertical lines in Figure 2. A detailed comparison of the lidar and the temperature profiles is presented in section 3.3.

3.2. Temperature Profiles During SCALE and ECHO and Comparison With Other Observations

In Figure 3 we show all falling sphere temperature profiles measured during SCALE (Figure 3a) and dur-

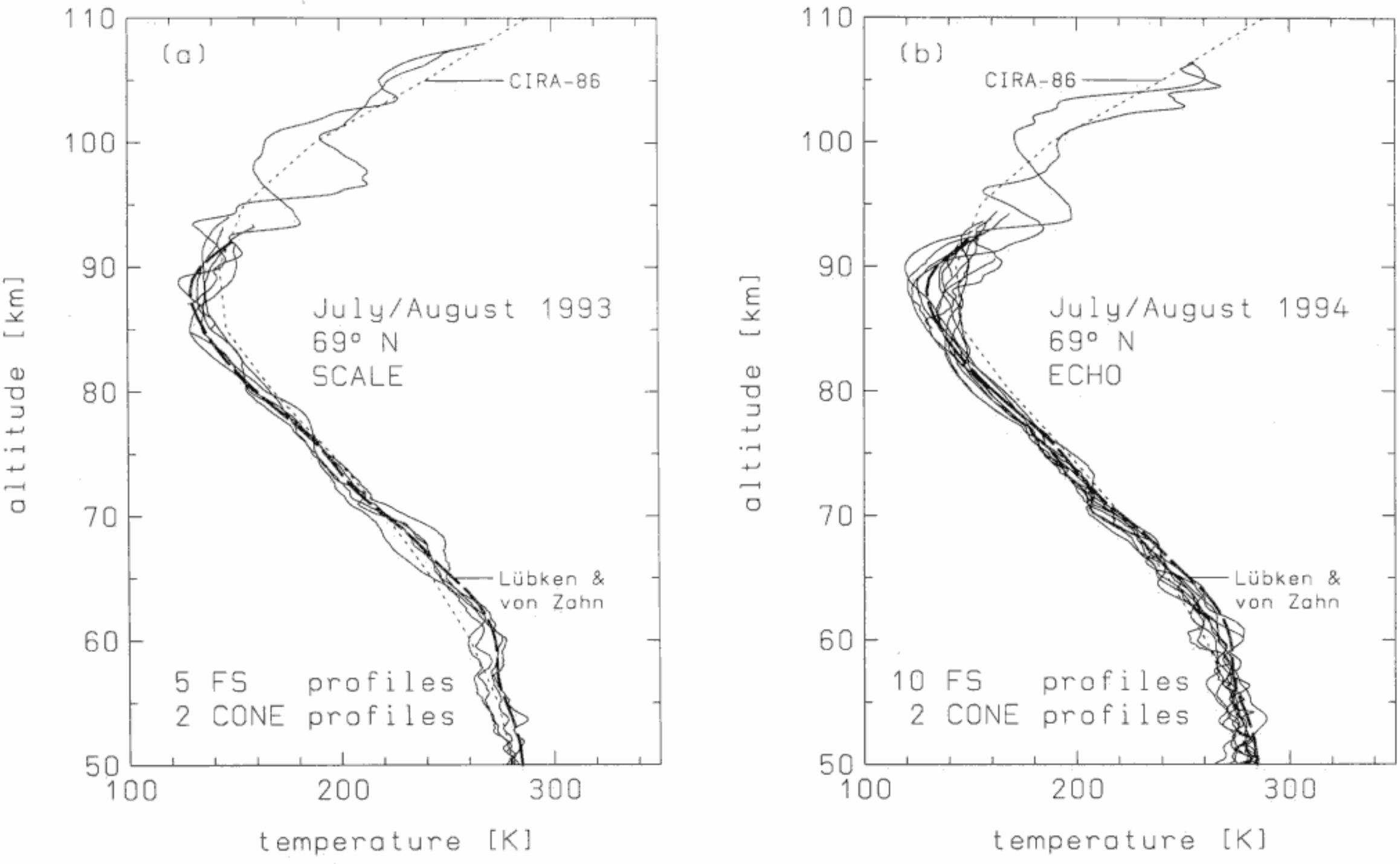

Figure 3. All temperature profiles measured by falling spheres and by CONE during (a) SCALE campaign and (b) ECHO campaign. For comparison we also show the CIRA (1986) profile for July at 70°N (dotted line). In addition, we have plotted the mean profile of our earlier measurements from 1986 for the month of July (thick dashed line) [*Lübken and von Zahn*, 1991].

ing ECHO (Figure 3b). In addition, the temperature profiles obtained by the CONE instruments are also shown [*Giebeler and Lübken*, 1995; *Lübken*, 1996]. The collection demonstrates that the thermal conditions in the upper mesosphere during the two campaigns were as expected for the summer season; very cold mesopause temperatures (around 135 K) at heights of typically 88 km [*Lübken and von Zahn*, 1991]. It also appears from Figure 3 that the variability is larger above ~84 km than below (we should keep in mind, however, the different spatial resolution of CONE and the falling spheres).

In Figure 4 we have plotted the smoothed mean of all 15 falling sphere profiles obtained during SCALE and ECHO. We have attributed this mean profile to "early August" since all flights were performed between July 28 and August 17. For comparison we show the CIRA (1986) July profile [*Fleming et al.*, 1990] and the mean profile for July of our earlier compilation of temperature measurements at polar latitudes [*Lübken and von Zahn*, 1991]. The comparison in Figure 4 shows that both profiles are very similar below the mesopause; in the entire mesosphere the difference between the two mean profiles is less than 6 K, and in the upper mesosphere the difference is even smaller (typically smaller than 2 to 3 K). The mesopause temperature in early August is 135 K, which is 5.5 K warmer than in July. This deviation is within the natural variability in either month but still may have an impact on the seasonal variation of NLC occurrence because of the critical dependence of supersaturation on temperature. The mean profile shown in Figure 4 supports our earlier statement [*Lübken and von Zahn*, 1991] that the thermal structure in the upper mesosphere is remarkably stable throughout the summer season. We have listed the mean temperature and density profiles in Table 3.

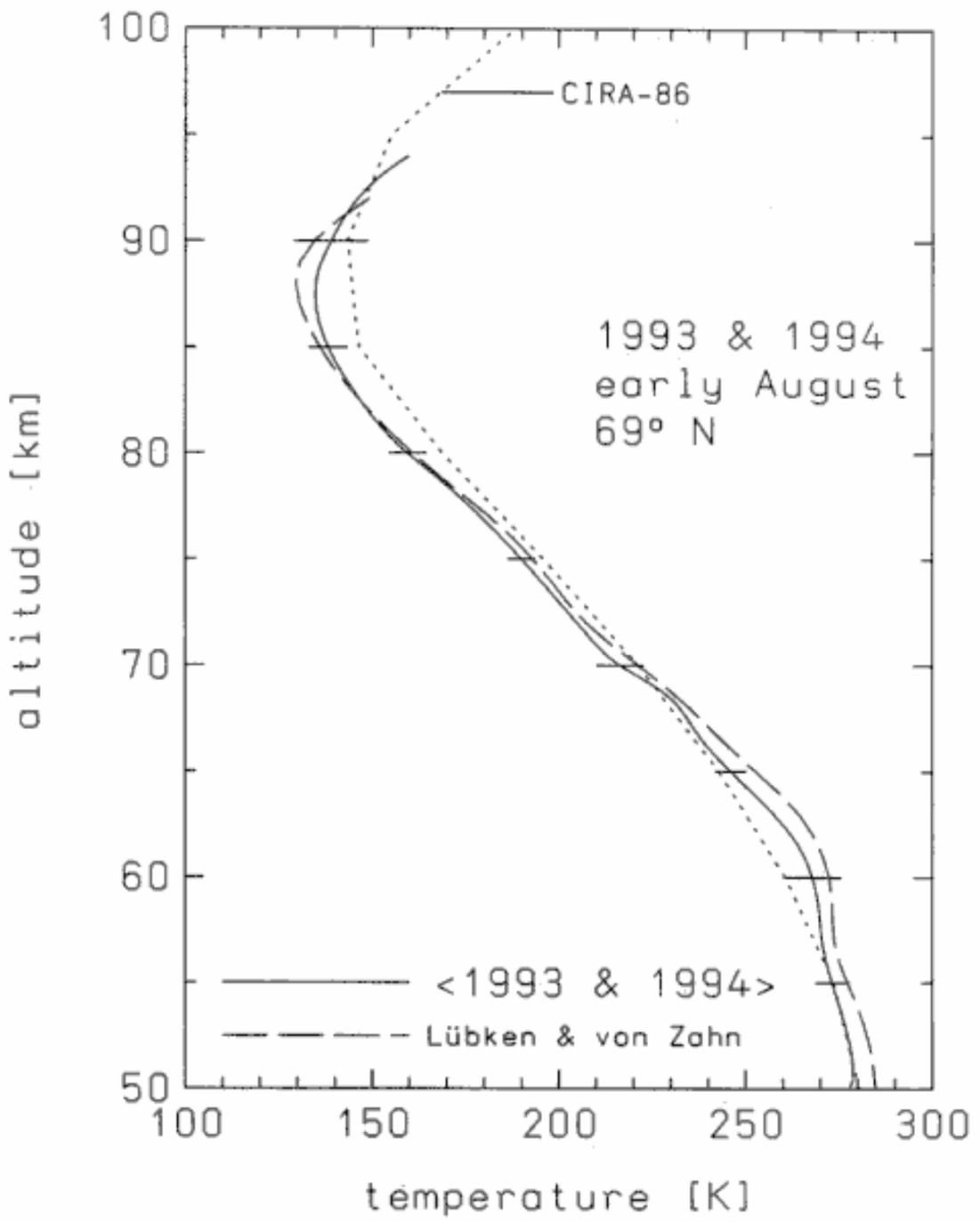

Figure 4. Mean of all temperature profiles measured by falling sphere during the SCALE and the ECHO campaigns. We have attributed this mean profile to early August since all flights were performed between July 28 and August 17. The horizontal bars show the variability. The CIRA (1986) profile (dotted line) and the mean of our earlier compilation (dashed line) for the month of July are shown for comparison [*Lübken and von Zahn*, 1991].

Table 3. Smoothed Mean Temperatures (T) of all 15 Falling Sphere Profiles From SCALE and ECHO

z km	T K	ΔT K	ρ kg/m^3	Number of flights
94	159.6	8.0	1.06E-06	3
93	151.7	6.6	1.42E-06	7
92	146.1	5.7	1.74E-06	10
91	142.1	7.5	2.22E-06	13
90	139.0	9.9	2.86E-06	14
89	136.3	9.5	3.74E-06	14
88	134.9	7.8	4.83E-06	14
87	134.9	6.9	6.14E-06	14
86	136.0	5.7	7.82E-06	14
85	138.2	5.2	9.88E-06	14
84	141.1	4.9	1.23E-05	15
83	144.7	4.5	1.51E-05	15
82	148.8	4.2	1.86E-05	15
81	153.5	4.5	2.24E-05	15
80	159.4	4.9	2.68E-05	15
79	166.3	5.3	3.16E-05	15
78	172.9	4.5	3.64E-05	14
77	179.0	3.0	4.23E-05	14
76	184.6	3.2	4.95E-05	14
75	189.9	3.7	5.77E-05	14
74	195.0	4.4	6.66E-05	14
73	199.9	4.1	7.70E-05	14
72	204.8	3.7	8.85E-05	14
71	209.8	4.4	1.02E-04	14
70	216.5	6.3	1.16E-04	14
69	225.9	7.3	1.29E-04	14
68	232.4	6.8	1.45E-04	14
67	236.3	5.7	1.65E-04	13
66	240.7	4.5	1.87E-04	13
65	246.1	4.1	2.10E-04	13
64	251.9	4.7	2.34E-04	13
63	257.5	3.6	2.61E-04	13
62	262.2	4.5	2.92E-04	13
61	265.7	5.3	3.27E-04	13
60	267.9	7.8	3.69E-04	13
59	269.2	3.8	4.15E-04	13
58	269.9	3.7	4.67E-04	13
57	270.5	4.2	5.31E-04	13
56	271.6	5.1	5.97E-04	13
55	273.2	4.5	6.72E-04	13
54	275.0	5.7	7.52E-04	13
53	276.6	4.6	8.49E-04	13
52	278.0	3.9	9.47E-04	13
51	278.7	3.8	1.07E-03	13
50	277.6	4.8	1.22E-03	13

Also listed are the temperature variability ΔT (RMS), the mean mass density ρ, and the number of flights contributing to the mean in each altitude z. The densities are given as mantissa and exponent, e.g., 1.06E-06 is 1.06×10^{-6}.

In the time period of April 23 until June 3, 1992, a total of 21 falling sphere flights were performed at the Andøya Rocket Range during the AEROSOL 1 campaign. We have used measurements after May 26 only (total of four profiles) since the earlier flights show wave-like disturbances that are typical for the winter season. The mean temperature of the remaining four profiles at 82 km is 152 K.

We now turn to the falling sphere temperature measurements during the AEROSOL 2 campaign in May 1995 at the Andøya Rocket Range. Again, we consider only the profiles measured after mid-May since the earlier profiles showed a much larger wave activity in the mesosphere typical for the winter season. From the four profiles measured in that period, three profiles are very similar, whereas the fourth profile showed a significantly colder mesopause (121.5 K) compared with the others (typically, 135 K). This profile was measured during the night of May 31 to June 1 and seems to be more typical for midsummer conditions. It has therefore been ignored when considering mean conditions in late May. The mean of the remaining three profiles in late May shows a mesopause temperature of 135 K at an altitude of 87 km. These values are, in fact, very close to our August mean discussed above, which suggests that both the late May and the early August period belong to the transition regime between winter and summer and vice versa, respectively.

3.3. Comparison of Temperature Profiles and NLC Observations

When comparing NLC altitudes and the temperature in the atmosphere, we assume that there is no significant horizontal variability in the thermal structure at scales of 40 to 50 km (which is the distance between the laser beam and the atmospheric volume probed by the falling sphere). In addition, we assume that the NLC layer is not significantly tilted over that distance. We will present a justification of this assumption in section 5.4.

A more detailed comparison of temperature profiles observed during the night of July 28–29 1993, in the scope of the SCALE campaign, is shown in Figure 5a. Profiles from two falling spheres (SCS02 and SCS04) and from the CONE instrument on board the TURBO payload SCT03 are shown. The two falling spheres were launched 16 min before and 15 min after the TURBO flight, respectively.

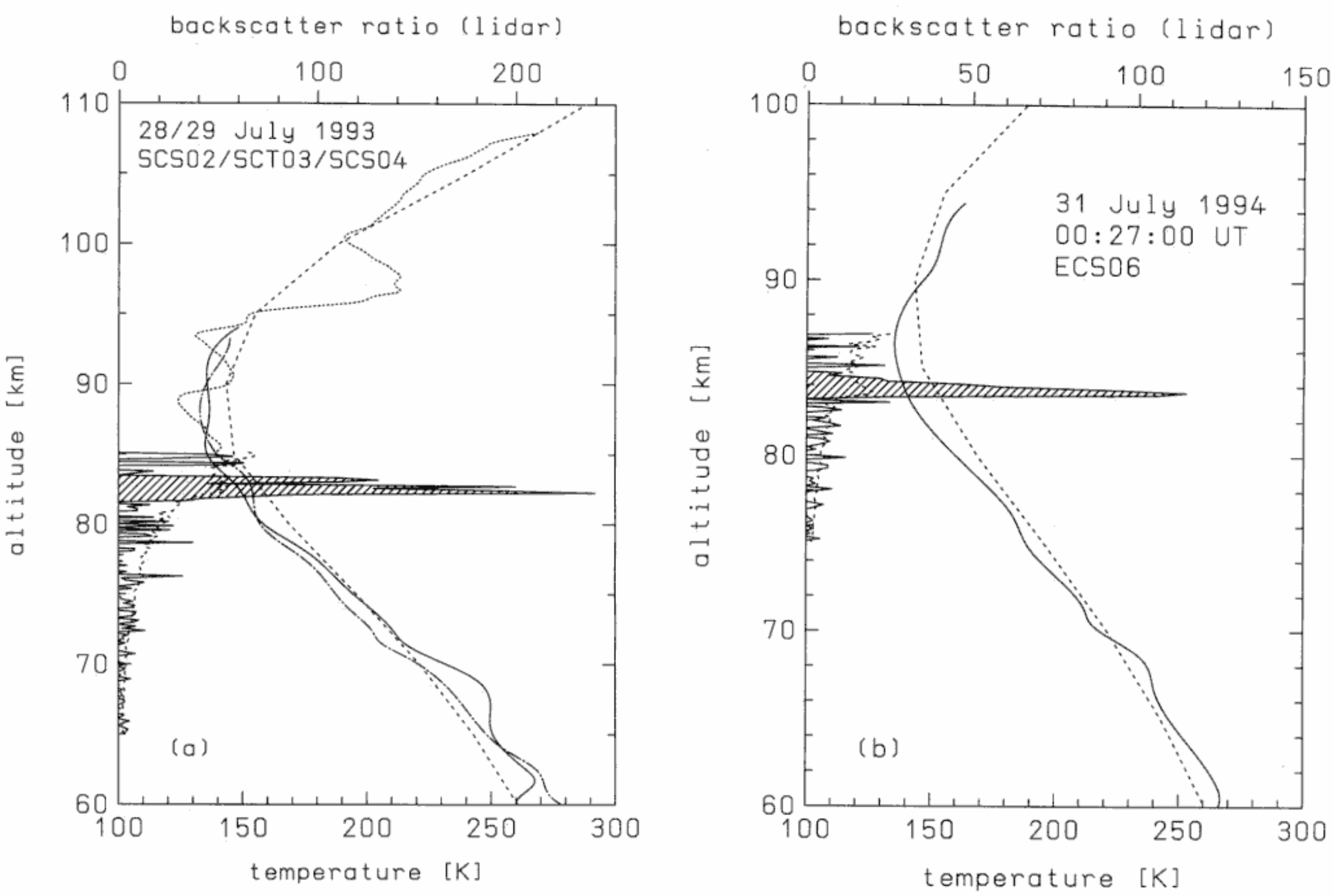

Figure 5. (a) Comparison of the temperature profile and noctilucent cloud altitude from the SCALE campaign. We have plotted the CONE profile (short-dotted line) and the falling sphere profile (solid line). The second falling sphere profile is plotted with a dash-dotted line. The flight labels are indicated. For comparison, the CIRA (1986) temperature profile for July at 70°N (long-dotted line) is shown. The hatched profile at the left ordinate (with the top abscissa being the corresponding x axis) shows the lidar backscatter ratio R obtained during the falling sphere flights together with the statistical noise signal.

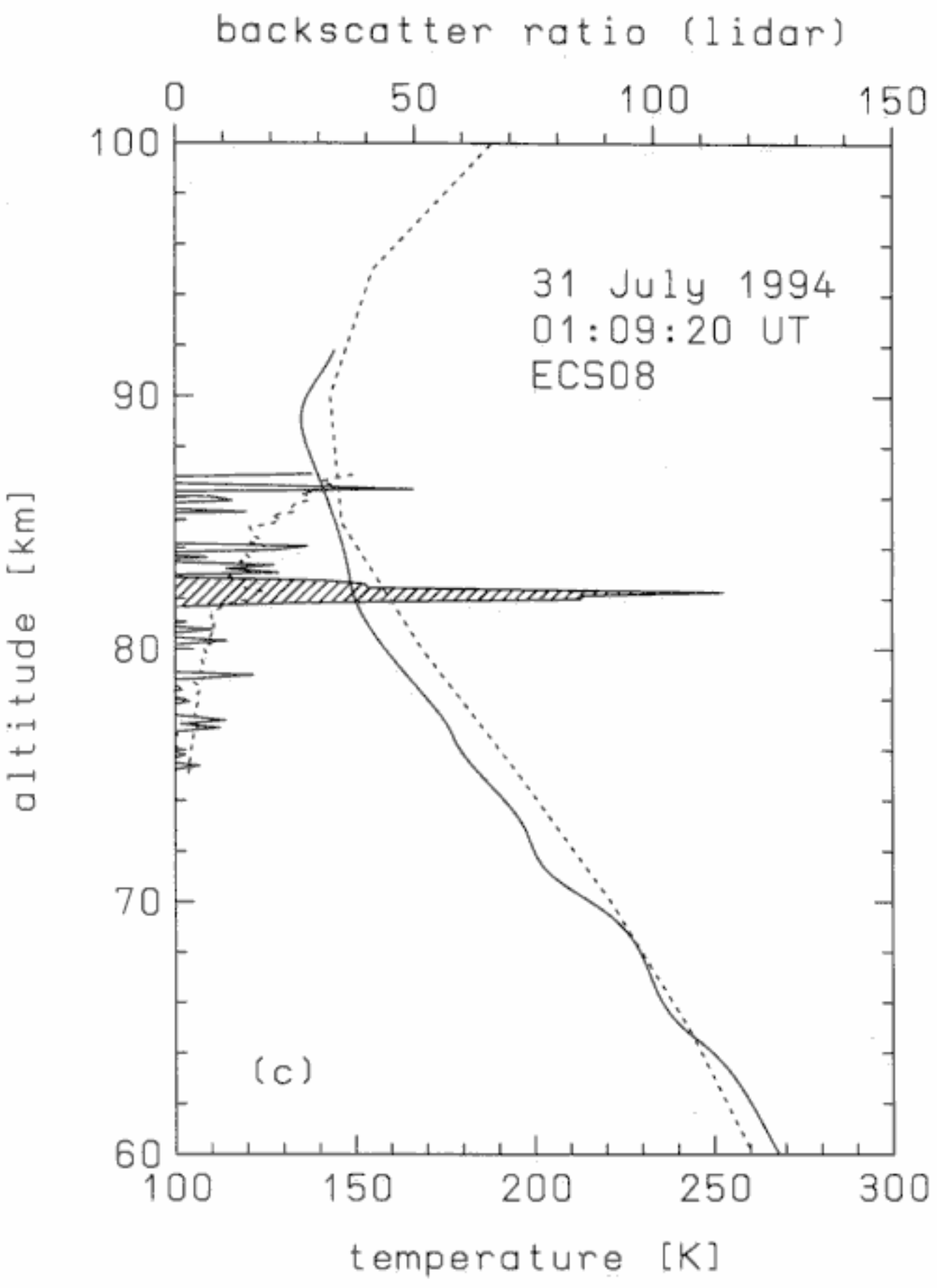

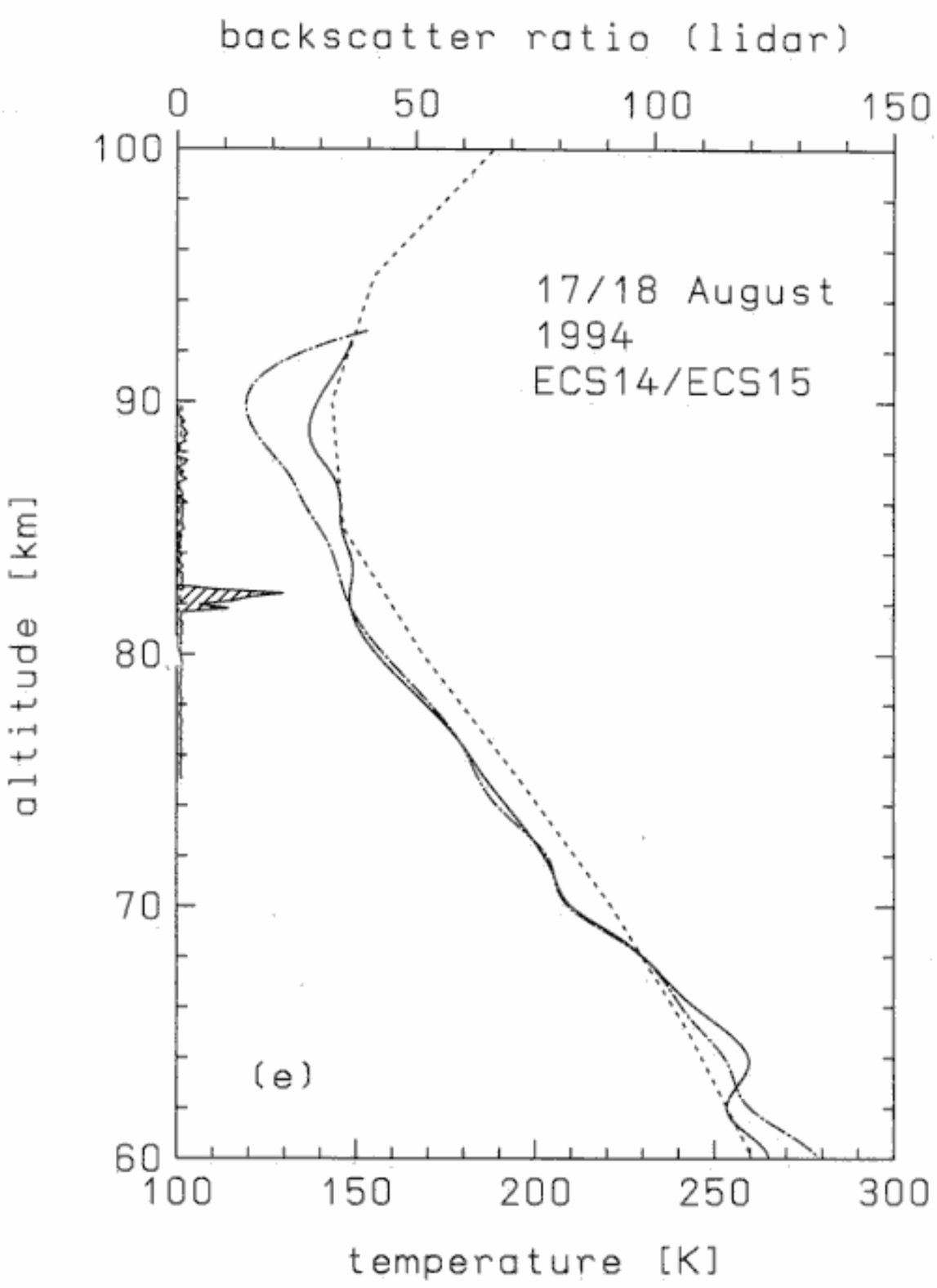

Figure 5. (continued)

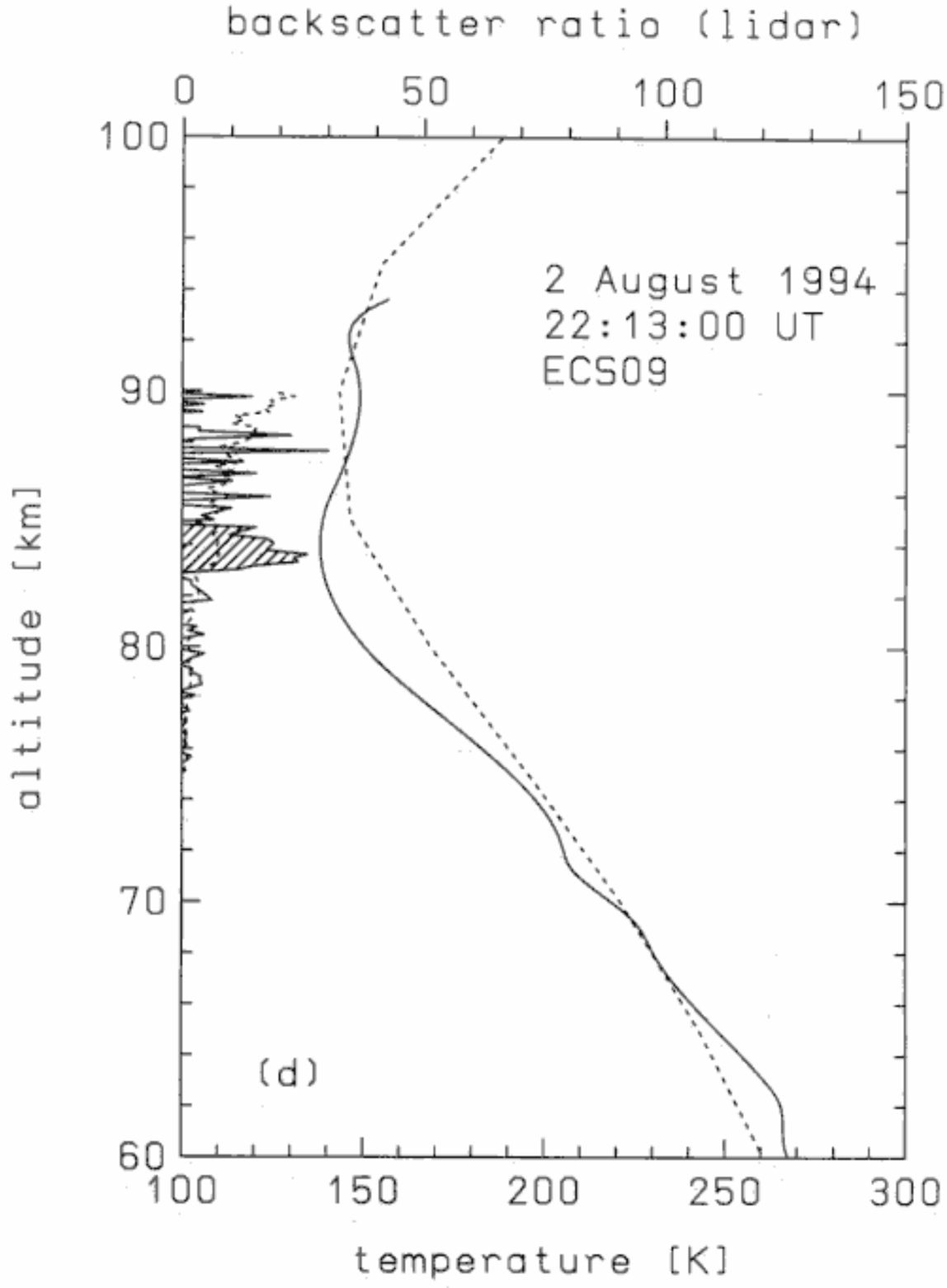

Figure 5. (continued)

The hatched profile at the left ordinate and the corresponding upper abscissa shows the backscatter ratio as measured by our lidar integrated from 2218 until 2236 UT. The maximum backscatter ratio of approximately 240 at 82.3 km corresponds to a Rayleigh equivalent altitude of 40 km, which is the strongest event in our record. Despite the poor observation conditions for the lidar and the corresponding incomplete time coverage during this particular night it can be seen from the time sequence of lidar profiles that the NLC layer did not change significantly in altitude near the falling sphere launches [*Langer et al.*, 1995a]. Since the two temperature profiles measured by the falling spheres are very similar, indicating stable thermal conditions, we have determined the temperature at the NLC layer from the mean of the two profiles. At the peak of the NLC layer, which is at an altitude of 82.6 km, the mean atmospheric temperature is 151 K. At the top and the bottom of the layer the mean temperatures are 147 and 153 K, respectively.

There were two more nights during SCALE with one successful falling sphere flight each; one during the night of July 26–27 and another during the night July 31 to August 1. NLCs were not observed in either night, even with favorable observational conditions for the lidar and in spite of a very low mesopause temperature.

During the ECHO campaign in 1994 there were 4 nights with NLC observations by lidar; we have performed temperature measurements with falling spheres

in three of them. The temperature profiles and the corresponding backscatter ratios of the lidar are shown in Figures 5b–5e. For the night July 30–31 1994, we show two temperature profiles (Figures 5b and 5c) since the lidar detected an NLC during both flights. As can be seen from these figures, the backscatter ratios vary significantly from case to case. Despite this variability there are some common features as follows: all NLC layers are located below the mesopause and the thickness of the layer is typically 1 to 2 km only.

The results deduced from all temperature and NLC observations shown in Figure 5 are summarized in Table 1. In the last three columns we have listed the altitude and the temperature of the NLC peak (if present) and the maximum backscatter signal within the layer. In order to classify the "sensitivity" of the lidar, we determine the altitude where the Rayleigh backscatter signal from atmospheric molecules approaches the noise limit ("max z" in Table 1). This altitude depends on instrumental and observational conditions, such as, e.g., background photons, integration time, tropospheric cloud coverage, etc. In order to describe the time coverage of the lidar observations, we have also listed in Table 1 the percentage of the time around the rocket flight ($\pm$ 1 hour) when the sky was sufficiently clear for the lidar to be capable of detecting NLCs with a backscatter ratio larger than 10.

4. Observations of NLC Height and/or Temperature: A Survey

The very first measurements of noctilucent cloud altitudes at the end of the last century by triangulation methods revealed that these clouds are located around 82 km [*Jesse*, 1891]. This was a surprise at that time since it was not expected that any constituent could condense or persist at that altitude. From a large set of photographic measurements the average altitude of the clouds was determined to be 82.08 $\pm$ 0.1 km [*Jesse*, 1896]. At that time, no technique was available to measure densities or temperatures in that part of the atmosphere. Many altitude observations of NLCs have been performed since then, however, most of the time without a simultaneous measurement of the atmospheric temperature profile at mesopause altitudes [see, e.g., *Witt*, 1962; *Taylor and Hapgood*, 1984].

The first temperature measurements around the mesopause in conjunction with NLC observations were performed in the early 1960s over Kronogård, Sweden (60°N) [*Witt*, 1968] and over Point Barrow, Alaska (71°N)[*Theon et al.*, 1967]. Extremely low mesopause temperatures ranging from 130 to 140 K near 85 km were observed by the rocket grenade technique, both with and without visually observed noctilucent clouds. It is interesting to note that no significant temperature difference was observed with the presence or confirmed absence of NLC. The drawback of these observations is that the height of the NLCs was not known.

A more precise determination of the NLC height was conducted with rocket-borne photometers in a summer campaign in 1978 from Esrange, Sweden (67°N) [*Björn et al.*, 1985]. A prominent increase of scattered solar light was observed at 82–84 km. The temperature at the cloud base as deduced from atmospheric rocket-borne Rayleigh scatter density measurements was found to be approximately 150 K, but with a rather large uncertainty of $\pm$ 10 K.

In summer 1982 the Cold Arctic Mesopause Program (CAMP) campaign was conducted at Esrange, Sweden [*Kopp et al.*, 1985]. During the night of August 3–4, 1982, throughout a period of NLC sighting from the ground, several sounding rockets were launched. The payloads were equipped with (among others) a positive ion probe, an ion mass spectrometer, the scattered light intensity profile sensor (SLIPS), and resonance fluorescence lamps to detect atomic oxygen. The SLIPS photometer detected an enhancement of scattered sunlight in the altitude range 82.4–83 km [*Wilhelm and Witt*, 1989]. The other instruments also detected striking features in this altitude range ($\sim$ 82.0–83.5 km), sometimes varying slightly between the upleg and the downleg of the rocket flight [see *Kopp et al.*, 1985, Table 3]. The time delay between the first and the last in situ detection of NLC was 33 min, and no significant change of the layer height was observed in this period. An active falling sphere was launched 11 min after the last in situ detection of NLC. This technique yields precise density and temperature information in the mesosphere and lower thermosphere, with an altitude resolution of approximately 100 m [*Philbrick et al.*, 1984]. A large-amplitude wave structure with temperature minima of 111, 119, and 138 K were observed at 93.6, 89.4, and 83.5 km, respectively, where the last coincides with the altitude of the NLC layer. The temperature profile was very smooth below ~83 km. The mesopause (smoothing over a wavelike feature) was found at 93.4 km with a temperature of 120 K. Since these measurements present the first unambiguous detection of NLC altitude and temperature, we have included these data in our analysis presented later.

The first detection of a noctilucent cloud by lidar took place during the night of August 5–6, 1989, at Andenes, Norway (69°N) [*Hansen et al.*, 1989]. From 2220 until 0010 UT a sodium lidar, detuned from the sodium resonance line by 5 Doppler widths, measured a significant backscattered signal in an altitude range 82.2–83.4 km. These data were later correlated with temperatures obtained from the same instrument [*Hansen and von Zahn*, 1994]. Unfortunately, these temperature data are limited to altitudes significantly above the NLC layer (86 to 94 km) due to the lack of sodium at NLC altitudes during summer.

In the scope of the NLC 1991 campaign a series of sounding rockets were launched during the night of August 9–10, 1991, from Esrange at times when an airplane observer reported a bright, persistent noctilucent cloud display [*Goldberg et al.*, 1993]. A particle and aerosol trap (PAT) instrument mounted on board a sounding rocket measured secondary electrons and ions released by impact of NLC particles in the alti-

tude range 82.75–83.5 km (peak at 83.1 km) on the upleg part of the flight [*Balsiger et al.*, 1993]. More than 2 hours (precisely 142 min) after this flight, another sounding rocket was launched and carried a SLIPS photometer that detected an enhanced scattered signal both on upleg (peak at 82.8 km) and on downleg (peak at 82.3 km) [*Zadorozhny et al.*, 1993]. These altitudes coincide nicely with the PAT measurement and indicate a very stable altitude for the NLC layer. In summary, there is strong experimental evidence from in situ measurements that the NLC layer was located at 82.6 ± 0.5 km altitude during this night, with very little height variation.

During this salvo a total of three falling spheres were launched successfully [*Schmidlin*, 1992]. We have reanalyzed these data in order to account for the temperature profile in the lower thermosphere as deduced from our TOTAL ionization gauge density measurements [*Hillert et al.*, 1994]. Here we have used the data from the first successful falling sphere flight only since it is the closest in time to the sounding rocket launches. Our analysis results in a mesopause height and temperature of 88.4 km and 110 K, respectively. At the NLC height of 82.6 km the atmospheric temperature is 150 K. It turns out that all three temperature profiles measured by falling spheres during this night are very similar; at the NLC altitude the variability of the temperatures is only ± 2 K, which is surprisingly small considering the time lag between the three launches (73 min between the first and the second flight and 96 min between the second and the third flight). These measurements suggest that the thermal structure was very stable during this night.

In summer 1993, two campaigns were conducted in northern Scandinavia, the SCALE campaign from Andøya (discussed previously), and the NLC 1993 campaign from Kiruna. In the scope of NLC 1993, two instrumented sounding rockets were launched during the night of August 2–3, 1993, at 0029 and 0102 UT, respectively. On this night, ground-based and airborne observers reported the presence of a NLC over the launch site. A particle impact sensor on board the first sounding rocket detected a NLC in the altitude range 83.0 to 83.6 km on upleg and in the range 85.6 to 82.5 on downleg [*Balsiger et al.*, 1996]. The instruments on board the second payload also detected conspicuous signals indicative of NLC particles, though at slightly lower altitudes near approximately 82 to 83 km (T. Blix and G.Witt, private communication, 1994). A total of four falling spheres were launched during this night, two of which followed the sounding rockets by only 8 and 22 min, respectively. The temperature profiles from these two flights are practically identical (within the instrumental error) and show a mesopause temperature of 130 K at 86.1 km (F. Schmidlin, private communication, 1994). The temperatures at the upper and lower edge of the NLC layer, i.e., at 85.6 and 82.0 km, are 130 K and 145 K, respectively.

The Rayleigh lidar at Aberystwyth (52.4°N) detected NLCs at comparatively low latitudes during four nights in the summer of 1993 [*Thomas et al.*, 1994]. Unfortunately, the enhanced backscatter by the NLC particles seriously compromises the derivation of temperatures at the NLC height. The upper limit for the mesopause temperature was estimated to be 137±7 K, deduced from the molecular backscatter profile measured before the occurrence of the NLC layer.

NLCs were also detected by lidar over Greenland (67°N) in late summer 1994 at altitudes between 80.6 and 85.0 km. During one night (August 15) a rather uncertain estimate of the mesopause temperature of 145 ± 15 K was deduced from the measured backscatter signal after integrating profiles for 3 hours [*Thayer et al.*, 1995]. In Table 4 we have summarized this survey of earlier attempts to simultaneously measure NLC altitude and temperature near the mesopause.

5. Discussion

5.1. Variability and Repeatability of the Temperature Below the Mesopause

The temperature profiles plotted in Figure 3 show that the geophysical variability is smaller below~84 km than above. For example, at 82 km the mean temperature of all 15 falling sphere profiles is 148.8 K and the variability (RMS) is only 4.2 K (see Table 5). It is interesting to note that the temperature at these altitudes shows a remarkable repeatability over the years. Even the very first temperature measurements performed during summer at latitudes northward of the polar circle more than 30 years ago over Kronogråd (66°N) and Point Barrow (71°N) showed very similar mean values at 82 km altitude, 150.6 and 148.7 K, respectively [*Theon et al.*, 1967; *Witt*, 1968]. The agreement between our mean temperature at 82 km and that of the early measurements is even more convincing since a different experimental technique ("rocket grenades") was used at that time, which allows one to determine temperature directly and not via density measurements. Again, a different technique ("active falling sphere") was used in one flight during the CAMP campaign in 1982 and, once more, gave a very similar result of 147.8 K at 82 km [*Philbrick et al.*, 1984]. A large set of 26 temperature measurements was compiled during the Middle Atmosphere Cooperation/Summer In Northern Europe (MAC/SINE) campaign in June and July 1987. Considering all 26 profiles, the mean temperature and its variability at an altitude of 82 km is 149.7 and 4.4 K, respectively [*Lübken and von Zahn*, 1991]. These values deviate by less than a degree from our 1993/1994 results presented in this paper. The NLC 1991 profiles published by *Schmidlin* [1992] again show a mean of 150.5 K and an even smaller variability of 1 K RMS (when considering variability, we should keep in mind, however, that the number of profiles and the time coverage can be very different from one data set to another).

The most recent temperature measurements close to the summer months were performed during the AEROSOL 2 campaign introduced in section 3.2. The mean of the four profiles obtained during late May 1995 gives a temperature of 149.3 K at an altitude of 82 km, again

Table 4. Literature Survey of Near Simultaneous NLC Altitude and Temperature Measurements

Campaign	Date	Site	NLC Height km	Technique	Temperature K	Technique
	July 29–30, 1963 Aug. 6–7, 1964 Aug. 15–16, 1964 Aug. 16–17, 1964	Kronogård	not known	visual	130–150 (at 82–88 km)	grenade
	Aug. 6–8, 1965	Point Barrow	not known	visual	130–140 K at 85 km	grenade
NLC	July 30, 1978	Kiruna	82 – 84	in situ	150±10 at base	photometer
CAMP	Aug. 3–4, 1982	Kiruna	82.4–83.5	in situ	144–137	active FS
	Aug. 5–6, 1989	Andøya	82.2–83.4	Na lidar	not known	
NLC	Aug. 9–10, 1991	Andøya	82–83.2	in situ	154–143	ionization gauge and FS
NLC	Aug. 2–3, 1993	Kiruna	82–85.6	in situ	145–130	FS

The campaigns and the techniques used to measure temperatures are explained in the text (FS is falling sphere and Na lidar is sodium lidar). The measurements during the SCALE and ECHO campaigns are listed separately in Table 1. Geographical coordinates of sites listed are Kronogård (Sweden), 66°N; Point Barrow (Alaska), 71°N; Kiruna (Sweden), 68°N; and Andøya (Norway), 69°N.

very close to our mean values listed above. The ALOMAR Rayleigh lidar was in operation during two of the four flights after mid-May but did not detect any NLC (G. von Cossart, private communication, 1995).

Could a tidal effect give rise to temperature variations larger than stated above? Most of the measurements referred to have been made around local midnight in order to optimize the viewing conditions for the ground-based observers and for the lidar. The majority of the other flights have been performed around local noon (e.g., 19 flights during MAC/SINE), which is at the same phase for the predominant semidiurnal tide. Models suggest that in the upper mesosphere at high latitudes the amplitude of the semidiurnal tide is only 2 to 3 K and the amplitude of the diurnal tide is even smaller [*Forbes*, 1982]. Such a small tidal modulation would have only very little impact on our mean temperature at 82 km.

The question arises whether this theoretical conclusion is supported by our data. An experimental answer to this question would require measurements at the opposite phase of the diurnal variation, i.e., at dawn and dusk. The closest measurements near these time periods were performed during the AEROSOL 1 campaign in late May 1992 (four flights at 1530 LT) and during the MAC/SINE campaign in June/July 1987 (two flights at 1512 LT and 2055 LT). Taking into account these six measurements, the mean temperature at 82 km is 149.8 K (± 4.5 K), which agrees nicely with the mean temperatures of the other campaigns. We conclude that the few profiles available do not indicate a strong tidal modulation of the mean temperature at 82 km, in agreement with the theoretical expectation stated above.

In Table 5 we have summarized the measurements of the mean temperature in summer and its variability at 82 km covering a time span of more than 30 years. The profiles within each data set have been averaged with equal statistical weight since only one technique is used within each data set, which implies that the error

Table 5. Temperature Measurements at 82 km Altitude During Summer at High Latitudes

Year	Location	Months	Number of Profiles	$\overline{T}^a$	ΔT, RMS	Source
1963/1964	Kronogård	July/Aug.	6	150.6	6.0	*Witt* [1968]
1965	Pt. Barrow	Aug.	4	148.7	2.5	*Theon et al.* [1967]
1982	Kiruna	Aug.	1	147.8	N/A	*Philbrick et al.* [1984]
1987	Andøya	June/July	26	149.7	4.4	*Lübken and von Zahn* [1991]
1991	Kiruna	Aug.	7	150.5	1.	*Schmidlin* [1992]
1992	Andøya	May/June	4	152.0	2.5	this paper
1993/1994	Andøya	July/Aug.	14	148.8	4.2	this paper
1995	Andøya	May	4	149.3	2.0	this paper

[a]Mean of $\overline{T}$ is 149.7 K and the RMS deviation is 1.2 K.

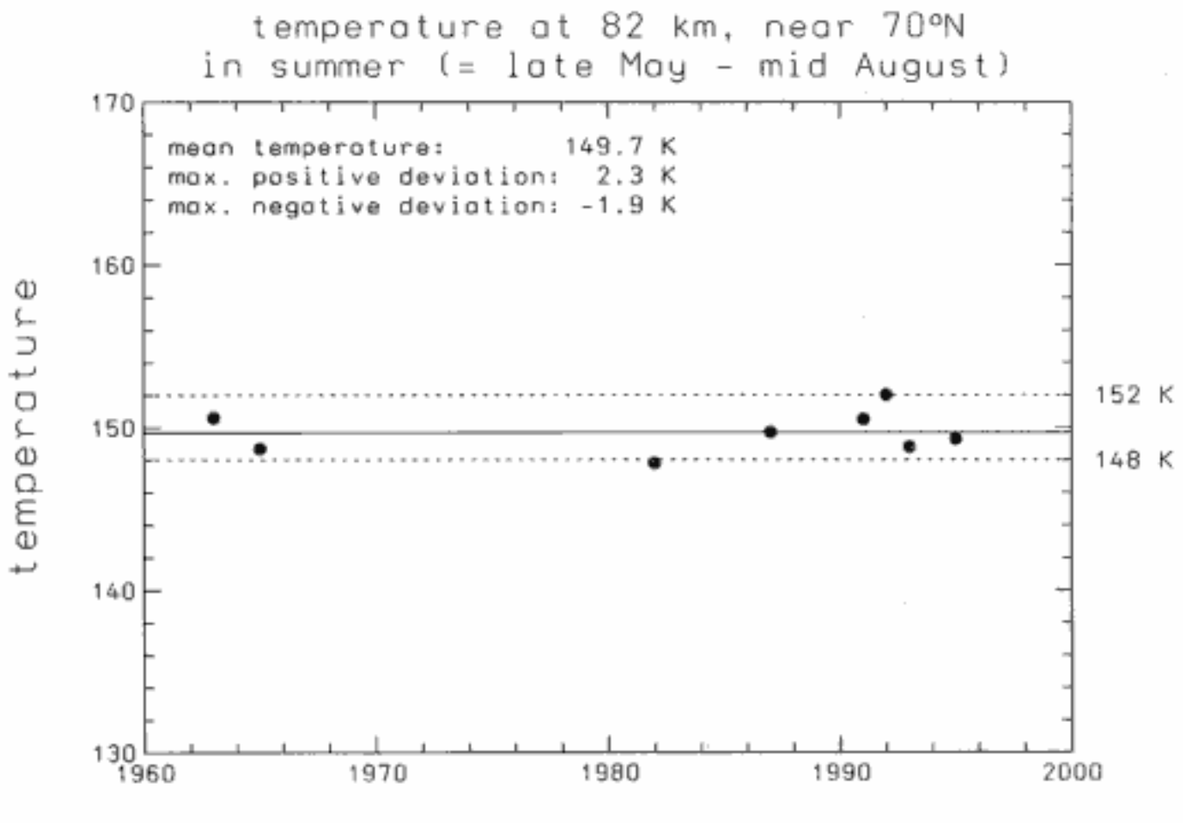

Figure 6. The mean temperature at 82 km in summer at a latitude of approximately 70°N (data from Table 5).

bars are approximately the same at a given altitude. The mean temperatures are plotted in Figure 6 as a function of time. We prefer not to plot the variabilities within each campaign since the number of profiles contributing to the mean value varies substantially from one data set to another (see Table 5). In summary, the mean temperature at 82 km in Arctic summer shows a remarkable repeatability within the last 30 years and was again and again observed to be very close to 150 K (the deviations from this value are within a range of ± 2 K). We suggest naming this effect "equithermal submesopause in summer".

With reasonable assumptions we can extend this statement to periods before the first temperature measurements in the 1950s; we assume that NLCs are observed by the naked eye most likely at an altitude where the particles are largest and that this altitude is critically determined by the degree of saturation S. This quantity is defined as the ratio of the actual to the saturation partial pressure of water vapor:

$$S = \frac{p_{H_2O}}{p_{sat}} = X \cdot \frac{p_{atm}}{p_{sat}} \qquad (2)$$

where $X = p_{H_2O}/p_{atm}$ is the volume mixing ratio of water vapor. The saturation pressure of water vapor over ice can be obtained from Kirchhoff's formula, the parameters of which have recently been updated [*Marti and Mauersberger*, 1993]:

$$\log_{10} p_{sat} = 12.537 - (2663.5/T) \qquad (3)$$

where p_{sat} is in Newtons per square meter and the temperature T is in Kelvins. As can be seen from these equations, the degree of saturation dramatically depends on temperature and, to a lesser extent, on the water vapor mixing ratio. For example, at 82 km a doubling of the water vapor content has the same effect on S as a decrease of the temperature by only 2.5 K. Since the altitude of the NLCs has repeatedly been reported to be between 82 and 83 km for more than 100 years, this implies that the temperature at these altitudes has not changed significantly. From the temperature data presented above we have direct experimental evidence for this conclusion, but only for the last 30 years.

There have been speculations in the literature about a systematic cooling in the upper summer mesosphere resulting in an increased occurrence rate of NLCs [*Gadsden*, 1990]. It has also been noted that an increase of water vapor caused by anthropogenically induced methane emissions would have a similar effect [*Thomas et al.*, 1989]. Our compilation of temperature measurements in this paper does not support the speculated -7 K in the last 20-30 years, at least not near 82 km. On the other hand, due to the larger variability and because of the limited number of profiles available at higher altitudes, we cannot make a similar statement for heights around the mesopause. It might well be that the temperature around the mesopause has changed in the last century and that this temperature is the critical factor limiting the formation of NLCs as is suggested from model calculations [*Turco et al.*, 1982; *Thomas*, 1995]. In any case our experimental result puts a serious constraint on any model prediction of secular changes of temperatures in the upper mesosphere. It is interesting to note that measurements and indirect hints at midlatitudes seem to suggest temperature changes in the upper mesosphere significantly larger than our results stated above [*Clancy and Rusch*, 1989; *Taubenheim et al.*, 1990; *Hauchecorne et al.*, 1991; *Offermann and Graef*, 1992].

5.2. Temperature in the NLC Layer

In Figure 7 we show the temperature in the peak of the NLC layer (crosses) and the temperature range throughout the entire layer (lines). We have included results from other campaigns as well. To the best of our knowledge, Figure 7 contains all data available on unambiguous and simultaneous measurements of NLC altitude and temperature. We have quietly assumed that the temperature of the NLC particles and the temperature of the atmospheric environment is identical, an assumption which requires justification. According to *Olivero and Bevilacqua* [1979], the particle temperature reaches a quasi-equilibrium value within times of the order of a few seconds but is generally different from its surroundings; below the summer mesopause the particles are systematically warmer then their atmospheric environment. However, since the difference is less than 3 K in the 80 to 83-km altitude range, our assumption stated herein seems reasonable.

As can be seen from Figure 7, the temperature in the layer in no case exceeds 154 K but can be as low as ~130 K. In Figure 7 we have also noted the altitudes of the NLC layers in order to emphasize that the colder layers appeared at higher altitudes.

5.3. Altitude and Temperature of the NLC Layer as Compared With Conditions at the Mesopause

In Figure 8 we show the altitude of the NLC layers and a comparison with the mesopause heights. It is

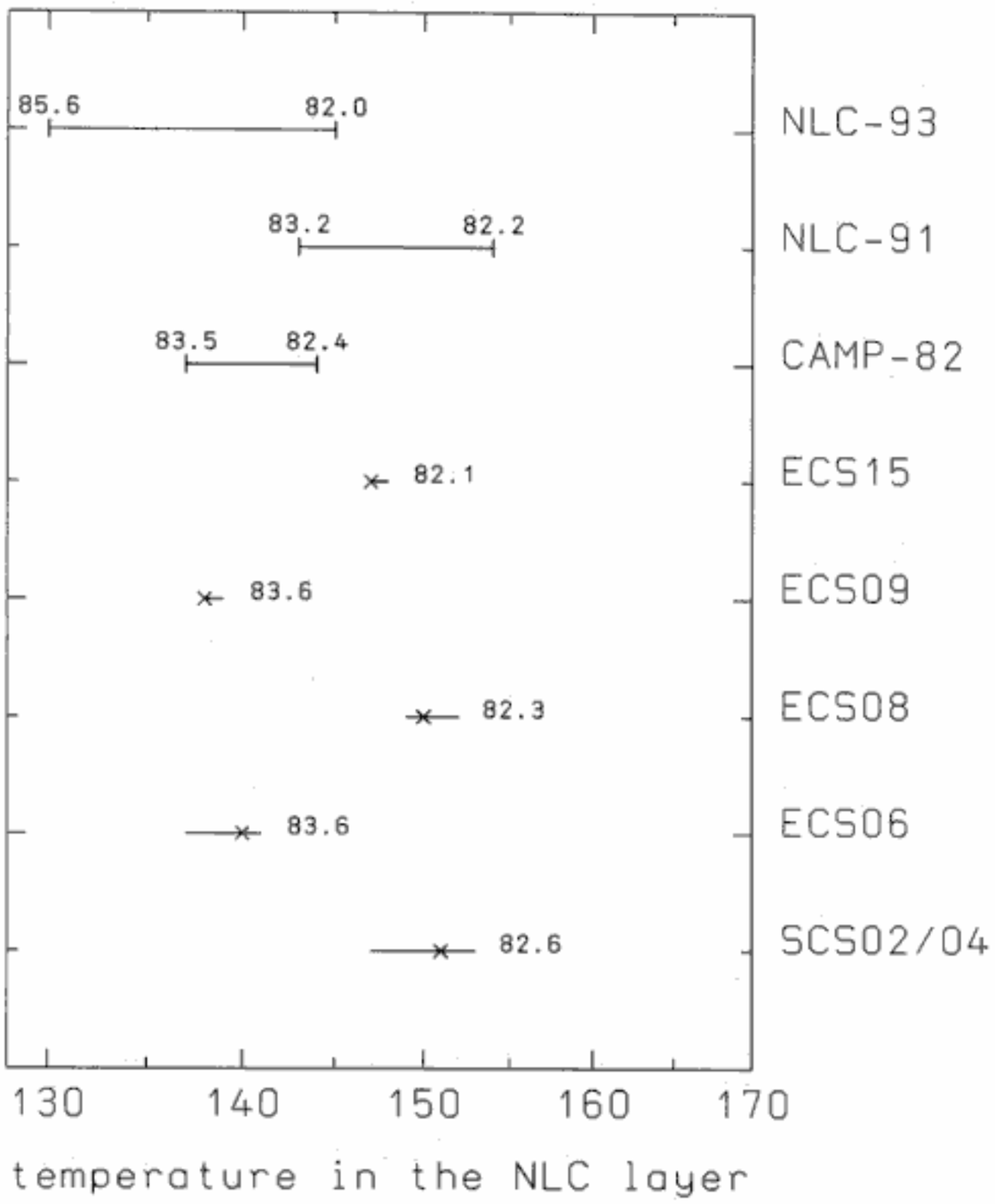

Figure 7. Atmospheric temperature in the noctilucent cloud (NLC) layer (crosses) and the altitude extent of the layer (lines). The falling sphere label for the SCALE and ECHO flights and the designation for the other campaigns are listed at right. The numbers beside each data point indicate the NLC altitude. For the data from the NLC 1993, NLC 1991, and CAMP 1982 campaigns, the altitude range is indicated above the temperature range.

interesting to note that the NLC layer (more precisely, the center of the layer) is in all cases located between 82 and 84 km. The mean peak altitude of all NLC layers observed by our lidar including profiles measured during the nights when no falling spheres were launched is 83.1 km. This mean was determined as follows: first, we calculated the average of the NLC peak altitudes in each night (the geophysical variability of the peak altitudes during 1 night is typically ± 1 km). Then we calculated the mean of the seven averages from each individual night. It turns out that the mean NLC height stated above is slightly biased toward large altitudes due to the weak but significant NLCs observed during the night of August 7–8, 1993, which extended to rather high altitudes of 87 km. Ignoring this one night results in a mean peak altitude of 82.8 km. These values are surprisingly close to the altitude of 82 km given by the very first observers more than 100 years ago [*Jesse*, 1896] (the unweighted mean of Jesse's data is 83.1 km, which is even closer to our result; the average deviation from the mean in Jesse's data is 1.8 km).

It clearly appears from Figure 8 that there is no obvious correlation between the altitude of the mesopause and the height of the NLC layer. Furthermore, the NLC layer is always located below the temperature minimum, except for the very low mesopause at 84 km during flight ECS09, which is a special case since the temperature profile exhibits a double mesopause in this flight (see Figure 5d).

Is there a correlation between the temperature at the mesopause and the occurrence of NLCs? In Figure 9 we show all mesopause temperatures measured during SCALE and ECHO. We have also marked whether or not a NLC was observed by the lidar during each flight (the size of the symbol indicates the quality of the observational conditions: the larger, the better). We should keep in mind that our classification of "no NLC" means that the lidar does not observe an enhanced backscattered signal in the upper mesosphere. The backscatter ratio, in turn, strongly depends on the radius of the aerosol particles ($\propto r^6$). As can be seen from Figure 9, a very cold mesopause is not a sufficient condition for enhanced lidar signals indicative for large NLC particles. For example, the falling sphere flights ECS01 and ECS03 showed a persistently cold mesopause of ~120 K at approximately 88 km, but the lidar did not detect any enhanced backscatter signal despite favorable observational conditions (Rayleigh equivalent height of 65 km). The above result is consistent with the sodium lidar measurements performed in August 1989, which demonstrated that the occurrence of this NLC depends only in part on the thermal condition above the display height [*Hansen and von Zahn*, 1994].

Is it interesting to note that all observed NLCs occurred at a mesopause temperature of ~135 K. Is this a fortuitous result? We do not see any mechanism that prevents particle coagulation at colder temperatures.

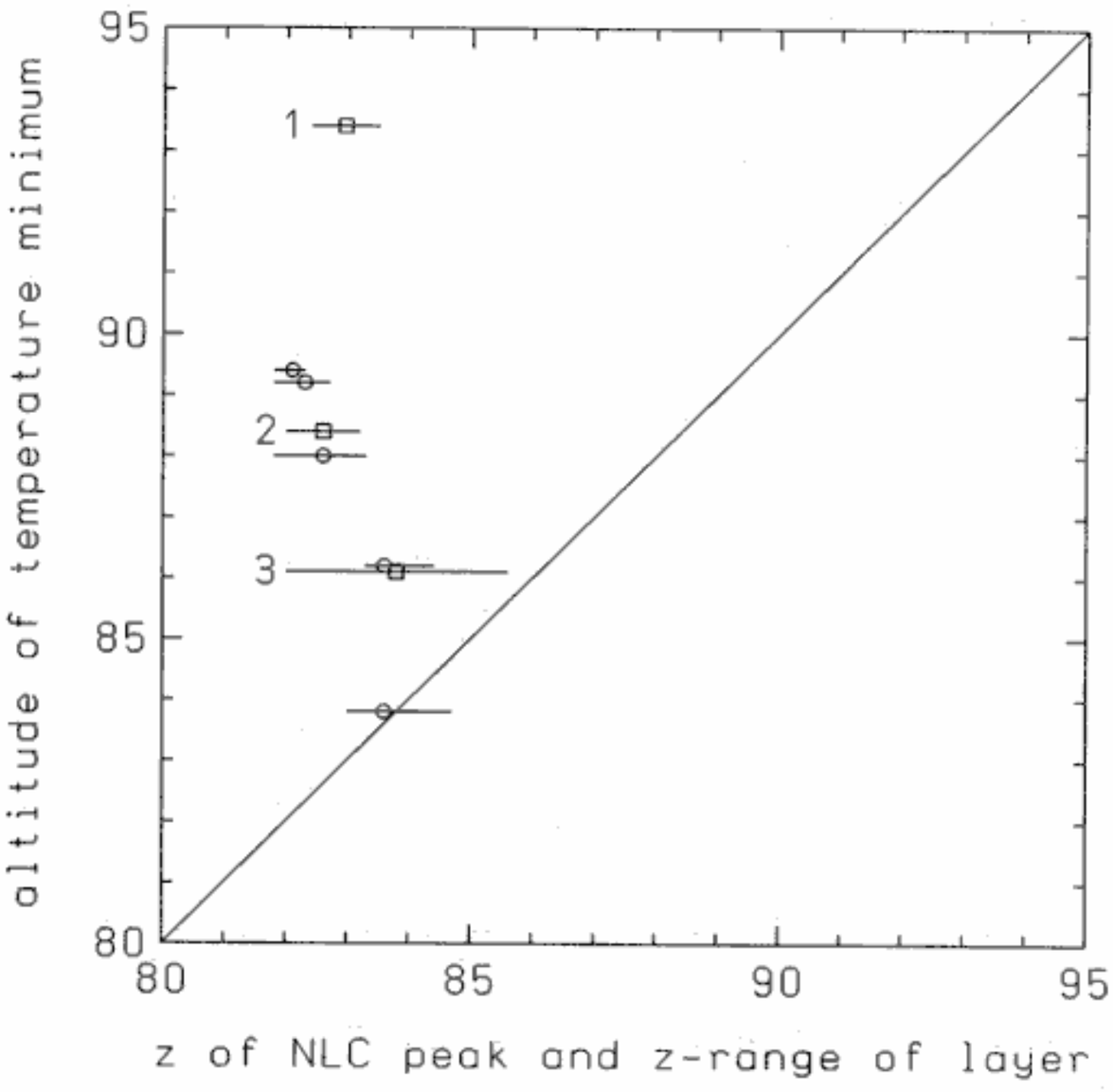

Figure 8. Altitude of the NLC peak (circles and squares) and altitude extent of the layer (lines) in comparison with the mesopause altitude. The data points labeled 1 to 3 are from the CAMP 1982, NLC 1991, and NLC 1993 campaigns, respectively. If the NLC were located around the mesopause, the data points should be grouped around the diagonal line.

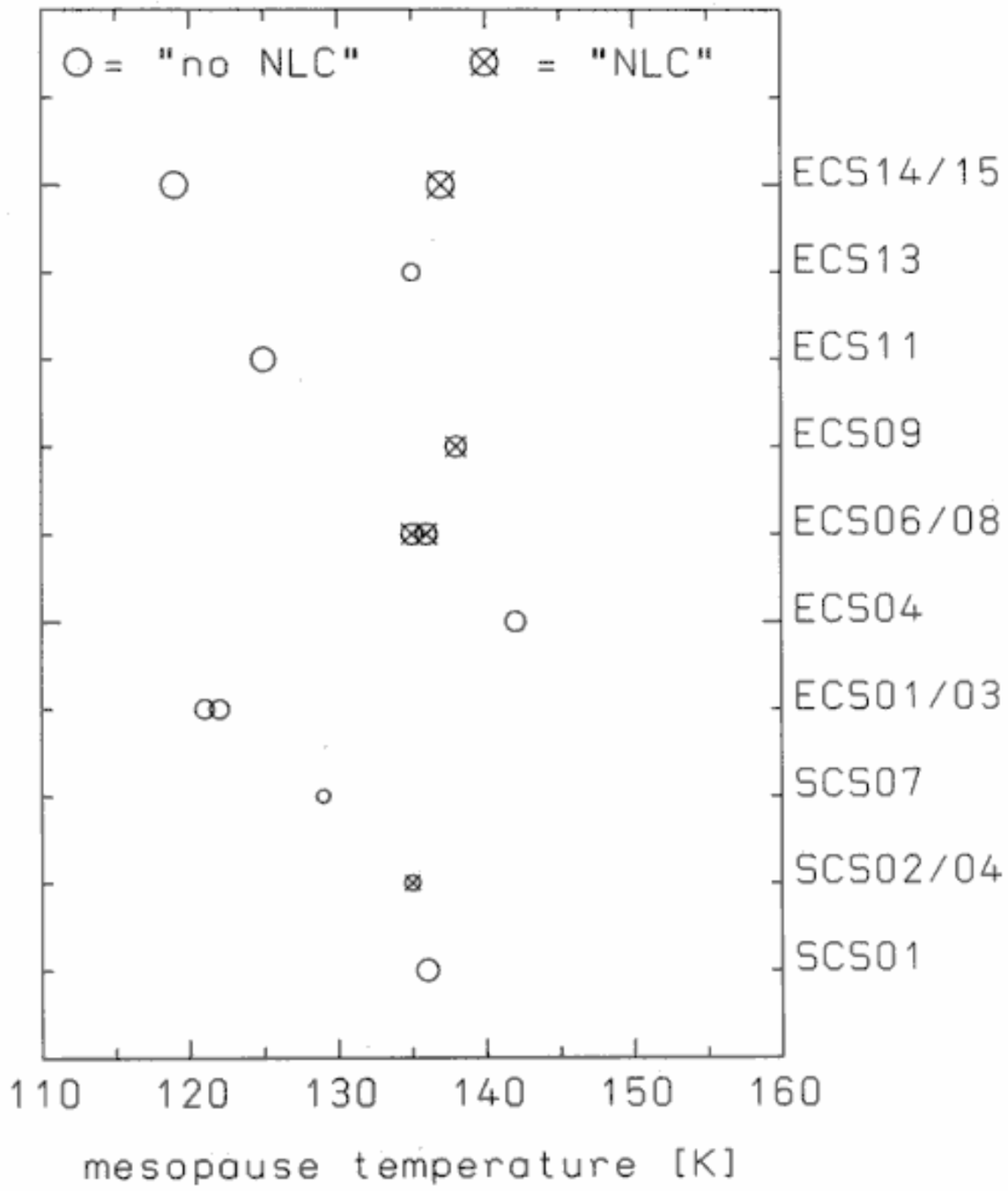

Figure 9. Mesopause temperature for all falling sphere flights during SCALE and ECHO. The falling sphere flight label is listed at right. The symbols indicate whether or not a NLC was observed by the lidar at the time of the flight or shortly before or after: an open circle means "no NLC", and a crossed circle means that an NLC was observed. The size of the symbols is a qualitative indicator of the observational conditions for the lidar: the larger, the better.

On the other hand, model studies suggest that at temperatures above 130 K dust nucleation is the dominant particle formation mechanism while at lower temperatures ion nucleation is more likely to occur. Dust nucleation leads to smaller concentrations of larger ice particles [*Turco et al.*, 1982] which are more easily to detect by our lidar than many small particles as generated by ion nucleation.

Is there any plausible reason for the noncorrelation between the conditions at the mesopause and the NLC occurrence at lower heights? It is interesting to look at the mean wind direction in the upper mesosphere as determined from the falling sphere measurements; below ~87 km the mean winds are blowing from the northeast (meteorological wind direction 60°), whereas the wind changes direction above that altitude. This experimental result agrees nicely with the more precise wind measurements at high altitudes during the MAC/SINE campaign in summer 1987 using the chaff technique [*Lübken et al.*, 1990]. Our observation implies that the air mass at mesopause altitudes stems from a different geographic location than the air mass at NLC altitudes and presumably has a different history concerning thermal conditions and humidity. It is therefore reasonable that there is no significant correlation between the conditions at the mesopause at the observation site and the appearance of NLCs at lower heights.

We can speculate about other possibilities that NLCs are not observed despite very low mesopause temperatures. For example, freeze drying during earlier times might have removed all the water vapor from the region. It could also be that a vertical and/or horizontal convergence of ice particles is required to produce an observable layer.

5.4. Particle Sinking Versus Layer Tilt

The temporal evolution of nearly all NLC layers observed so far by our lidar has shown a remarkable decrease in the altitude of the signal as a function of observation time. Speculating that this decrease is due to a settling of the NLC particles, we have estimated the settling speed and the size of the particles. For example, the lidar observation of the NLC event from July 31, 1994, shows an apparent decrease of the layer by approximately 2 km/h after 0030 UT (see Figure 2). Assuming spherical ice particles and using the density and temperature measurements of the falling spheres ECS06 and ECS08, this settling speed requires a particle radius of ~300 nm [*Fogle and Haurwitz*, 1966]. In the case of the NLC event from August 17, 1994, the stronger layer tilt observed by the lidar yields a settling speed of 2.5 km/h and a particle radius of 425 nm (in this case we have used the data from flight ECS15). We would arrive at even larger radii if the particles were nonspherical [*Reid*, 1975]. Particle radii of 300 nm and above are very unlikely for mesospheric cloud particles, referring to models [*Turco et al.*, 1982] or to estimates from satellite measurements [*Thomas and McKay*, 1985].

Could it be possible that the NLC layer is tilted and that the horizontal drift of the layer through the laser beam fakes a downward motion of the layer? Using the horizontal wind speed of 60 m/s as measured by ECS06 and ECS08 around 83 km, the layer would have to be tilted by only 1 km per 100 km in order to explain the 2 km/h apparent sinking of the NLC layer (to be more precise, this tilt is the projection of the direction of the real tilt to the direction of the cloud motion). This tilt is certainly within the range of possibilities and is compatible with results from upleg/downleg data of rocket-borne detection of NLCs [*Zadorozhny et al.*, 1993].

On the other hand, assuming that any horizontal inhomogeneity at scales of a few hundred kilometers is caused by a stochastic process (e.g., by phase variations of gravity waves), one would expect a random distribution of tilt angles and thus expect to observe "sinking" and "rising" layers. However, nearly all NLC layers observed so far by lidar have shown an apparent downward motion or have been steady in altitude; very seldom has there been an observation of an apparent upward motion [*Hansen and von Zahn*, 1994; *Thomas et al.*, 1994; *Thayer et al.*, 1995; *Langer et al.*, 1995b; Nussbaumer et al., submitted manuscript, 1996]. There is another geophysical phenomenon called polar mesosphere summer echoes (PMSE) that is closely related to aerosol

particles and which is observed much more frequently than NLCs (cf. review by *Cho and Kelley* [1993]). These PMSE layers again and again show apparent downward drifts with approximately the same rate as our NLC layers of 1 to 2 km/h [*Cho et al.*, 1993; Nussbaumer et al., submitted manuscript, 1996]. These data therefore confirm our observation that the tilts of the layers (if any) are not randomly distributed.

In summary, we conclude that it is very unlikely that the observed apparent downward motion of the NLC layers is simply caused by a physical settling of the particles. It seems more likely that the particle sinking is caused by vertical winds in the atmosphere, induced, e.g., by gravity waves. In addition, we cannot positively exclude that the layers are tilted and that they are drifting through the vertical laser beam.

5.5. Consequences of the Temperature Profile for the Degree of Saturation

We now discuss the consequences of the temperature profiles shown in Figure 5 for the presence of ice particles, which are presumably the cause of the lidar aerosol echoes and NLC displays in general. The evolution of an existing ice particle depends on the degree of saturation S for water vapor; if $S > 1$, the particle will grow, and if $S < 1$, it will evaporate. Equations (2) and (3) reveal that the saturation pressure of water vapor over ice and thus the degree of saturation determining the fortune of the NLC particles critically depend on temperature. The problematic quantity in this context is the actual amount of water vapor present in the atmosphere. Unfortunately, water vapor measurements in the upper mesosphere are very difficult to perform, and no observations have been made during our campaigns. Therefore we have to make assumptions concerning the water vapor mixing ratio profile at the altitude of interest. Model calculations and empirical reference atmospheres (based on very few measurements in the upper mesosphere) suggest that the water vapor mixing ratio at 85 km in summer is somewhere between 0.1 and 3 parts per million by volume (ppmv) [*Garcia*, 1989; *Smith and Brasseur*, 1991; *Russel*, 1987]. Note that one cannot derive an atmospheric H_2O mixing ratio from the lidar aerosol measurements, because NLC particles have swept up water vapor from a large volume of air while sedimenting ("freeze drying").

In Figure 10 we show altitude profiles of the degree of saturation for a water vapor mixing ratio of 0.1, 0.3, 1, and 3 ppmv, respectively, using the measured tempera-

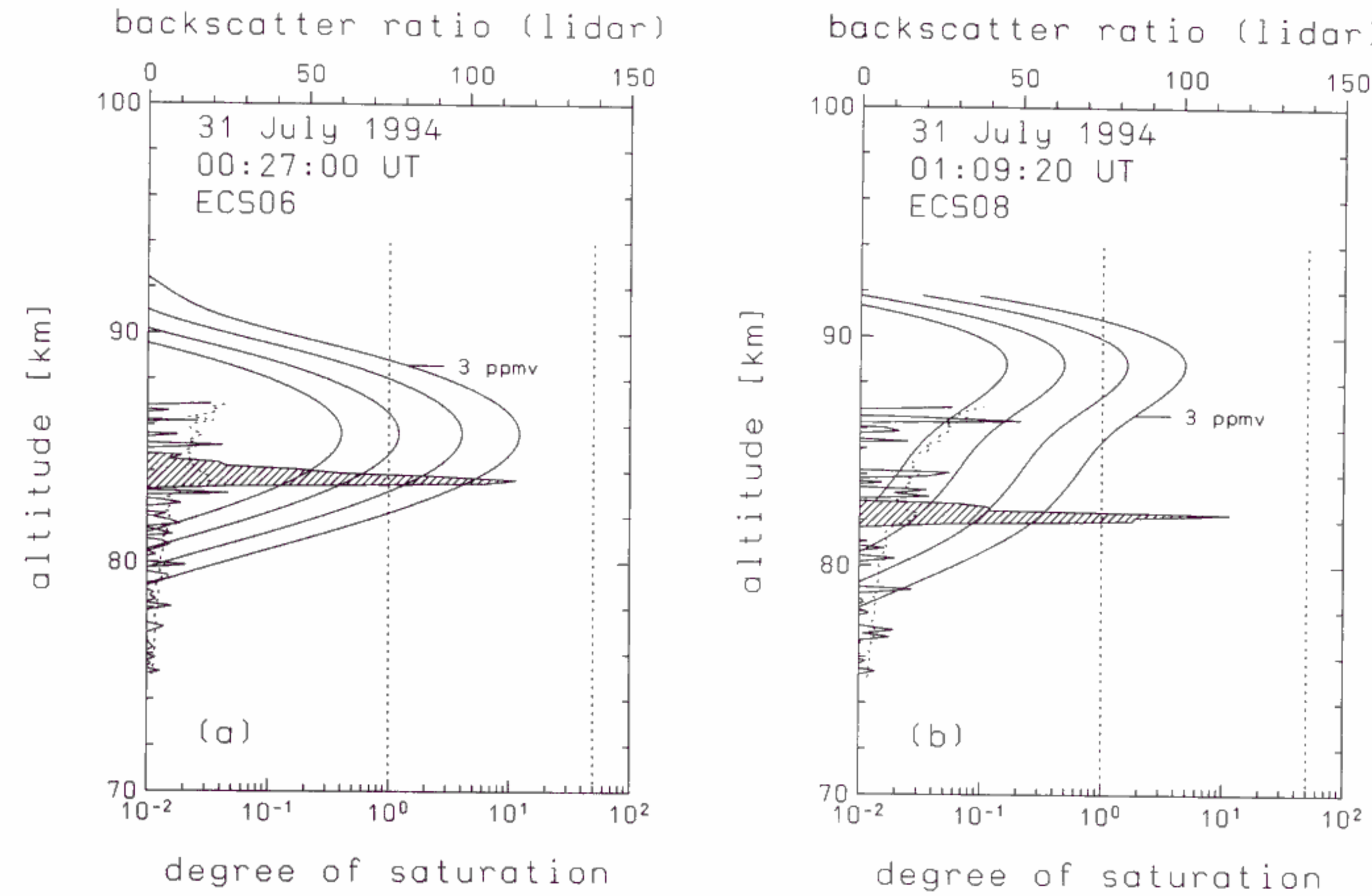

Figure 10. The degree of saturation S derived from the temperature profile of falling sphere flights (a) ECS06 and (b) ECS08, assuming water vapor mixing ratios of 0.1, 0.3, 1, and 3 ppmv, respectively, being constant with altitude. The backscatter ratio of the lidar is also shown (at the left ordinate and corresponding abscissa at the top x axis). The dotted lines mark the critical values for supersaturation ($S = 1$) and for the degree of saturation required to initiate nonhomogeneous nucleation (see text for more details).

ture profiles from flight ECS06 (Figure 10a) and flight ECS08 (Figure 10b). In the temperature minimum of the ECS06 profile at 86.2 km a water vapor mixing ratio of 0.1, 1, and 3 ppmv leads to a degree of saturation of 0.4, 4, and 11, respectively. At the altitude of the NLC layer the degree of saturation is larger than unity only for water vapor mixing ratios larger than ~1 ppmv. It is interesting to note that the degree of saturation is nowhere large enough to allow for homogeneous nucleation or nucleation on a singly charged ion which requires S to be larger than ~50 [*Gadsden and Schröder*, 1989]. Before we draw any premature conclusions, we should keep in mind that the initial creation of the ice particles most likely occurred some hours before our observations when the air parcel was hundreds of kilometers away [*Jensen and Thomas*, 1988]. The thermal structure at that time and place was most likely different from what we observe. Our measurements only allow conclusions about the status of the atmosphere at the time of observation, not about the history of particle growth, etc.

The temperature profile of flight ECS08 results in values for S at the NLC altitude which are smaller than unity, even for a water vapor mixing ratio of 3 ppmv, which implies that the particles are evaporating (see Figure 10b). How long does it take for a particle to disappear in this environment? The rate of change of the size of ice particles due to evaporation and condensation is most sensitive to the degree of saturation, thus on the temperature and the humidity of the atmosphere. Using the equation presented by *Gadsden* [1981], we have calculated the time required for a particle with a radius of 50 nm to evaporate (see this reference for a discussion on the assumptions and the limitations on using this equation). The results for the evaporation time are shown in Figures 11a and 11b for flights ECS06 and ECS08, respectively. In the case of ECS08 the time required for a particle to evaporate is approximately 1 to 3 hours, which is in rough agreement with the fact that the NLC disappeared shortly after the ECS08 launch (see Figure 2). On the other hand, we cannot positively exclude that the cloud drifts out of the field of view of the lidar simply because of its limited horizontal extent.

The variability of temperatures at the NLC layer corresponds to an even larger variability of the degree of saturation S; for a water vapor mixing ratio of 1 ppmv (a value most favored by the models at around 82–85 km) we find values for S varying by almost 3 orders of magnitude between 0.05 and 50 (including the results from CAMP, NLC 1991, and NLC 1993).

We have stated already that a low enough mesopause temperature is not a sufficient condition for the appearance of a NLC. A different way of demonstrating this experimental fact is to look at the degree of saturation at the mesopause and compare this with the occurrence of NLCs. The results of these calculations are shown in Figure 12 for all falling sphere flights performed during SCALE and ECHO. Again, there is no obvious rela-

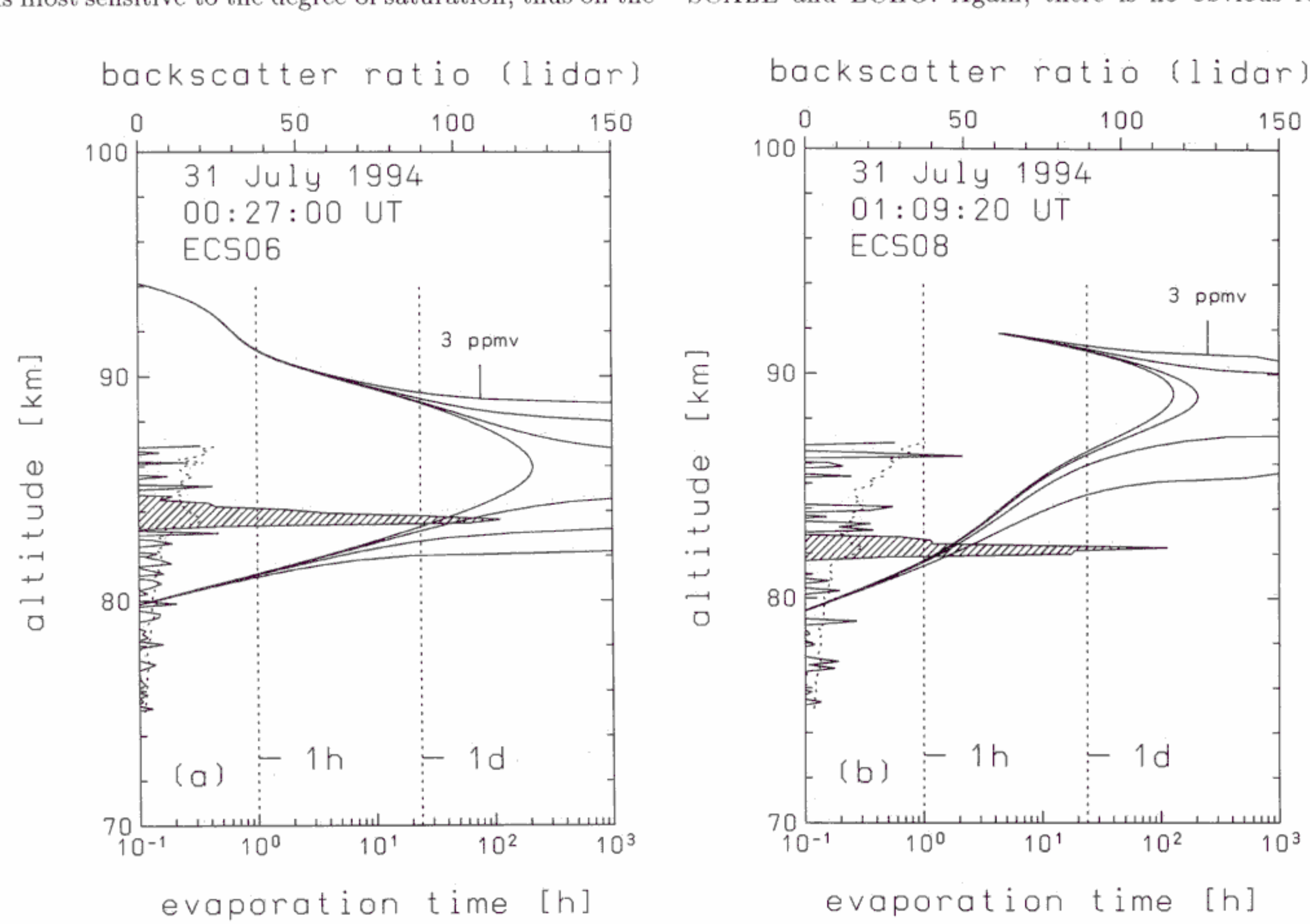

Figure 11. Same as Figure 10, but for the evaporation time of a particle with a radius of 50 nm. (a) is for ECS06, and (b) is for ECS08.

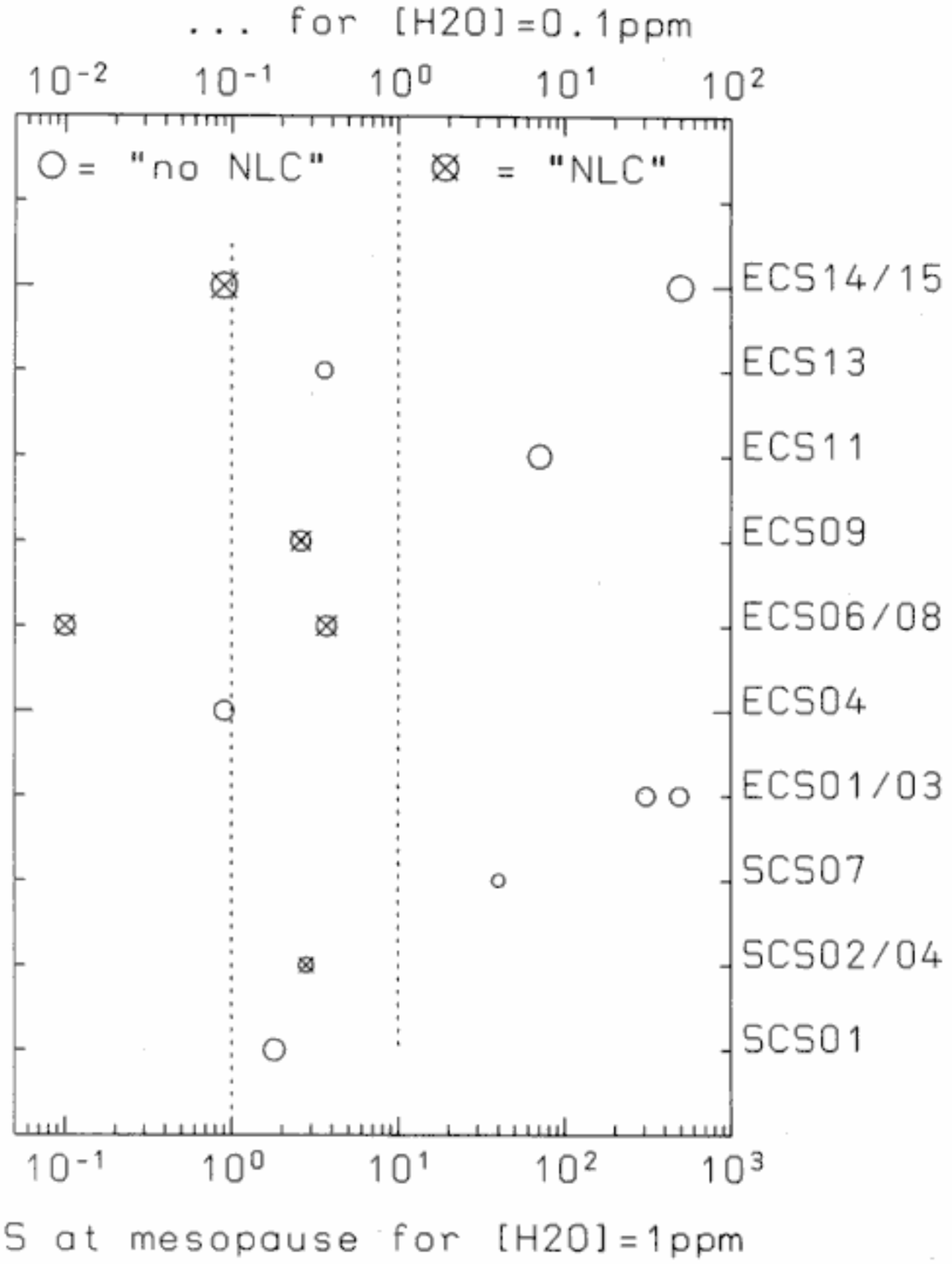

Figure 12. As in Figure 9, but for the degree of saturation S at the mesopause assuming a water vapor mixing ratio of 1 ppm (bottom abscissa) and 0.1 ppm (top abscissa), respectively. The critical values of $S = 1$ are marked by the dotted lines.

tionship between the appearance of NLCs and the degree of saturation around the mesopause; sometimes no NLCs are observed, even when the degree of saturation is very high at the mesopause (e.g., in the case of ECS01/03). This observation demonstrates that a cold enough mesopause temperature does not control alone whether or not NLC nuclei can grow to sufficiently large particles to be seen by the lidar from the ground. Considering our discussion at the end of section 5.3, it seems likely that this noncorrelation is at least in part due to horizontal and/or temporal inhomogeneities resulting in different histories of the air masses at the mesopause and at NLC heights, respectively.

5.6. Mean Conditions and Seasonal Variation

In order to elucidate the mean conditions during our campaigns in terms of the conditions for particle growth, we show in Figure 13 a segment of the mean temperature profile of Figure 4 and the resulting profiles for the degree of saturation S assuming a water vapor mixing ratio of 1 ppmv (since the degree of saturation scales with humidity, one can easily read values for S from Figure 13 for mixing ratios other than 1 ppmv). For the mean condition during our campaign, particles can grow (i.e., $S > 1$) at the mesopause only if the water vapor concentration is larger than 0.3 ppmv. On the other hand, in order to achieve values for S larger than 50 (a typical value required to initiate nonhomogeneous nucleation), the water vapor content would have to be 30 ppmv or, which may be more realistic, the temperature would have to be approximately 6 K lower than the mean temperature. Such a temperature drop is certainly within the natural variability observed at these altitudes (see Table 3). Please note that the mean temperature profile of late May is very similar to that of early August and that therefore our conclusions from above also hold for late May.

In Figure 13 we have also plotted the mean temperature profile for July from our earlier compilation [*Lübken and von Zahn*, 1991] and the corresponding curve for S. The fact that the mesopause is colder by 5.5° results in supersaturation values larger by a factor of 6 compared with our mean for early August and for late May. We therefore conclude that the mean mesopause temperature varies only by a few degrees from late May until mid-August. The satellite observations of the frequency of PMC occurrence at high latitudes show a rather sudden onset and termination in late May and mid-August, respectively [*Thomas*, 1984] (a comparison with ground-based NLC statistics is more difficult due to the unfavorable viewing conditions at high latitudes). As we have shown above, this seasonal variation is related to an abrupt change of the thermal structure in late May and in mid-August.

6. Conclusions

We have presented new simultaneous measurements of the thermal structure in the mesosphere by falling spheres and the altitude of the NLCs by lidar. The observations were performed at polar latitudes (69°N) in

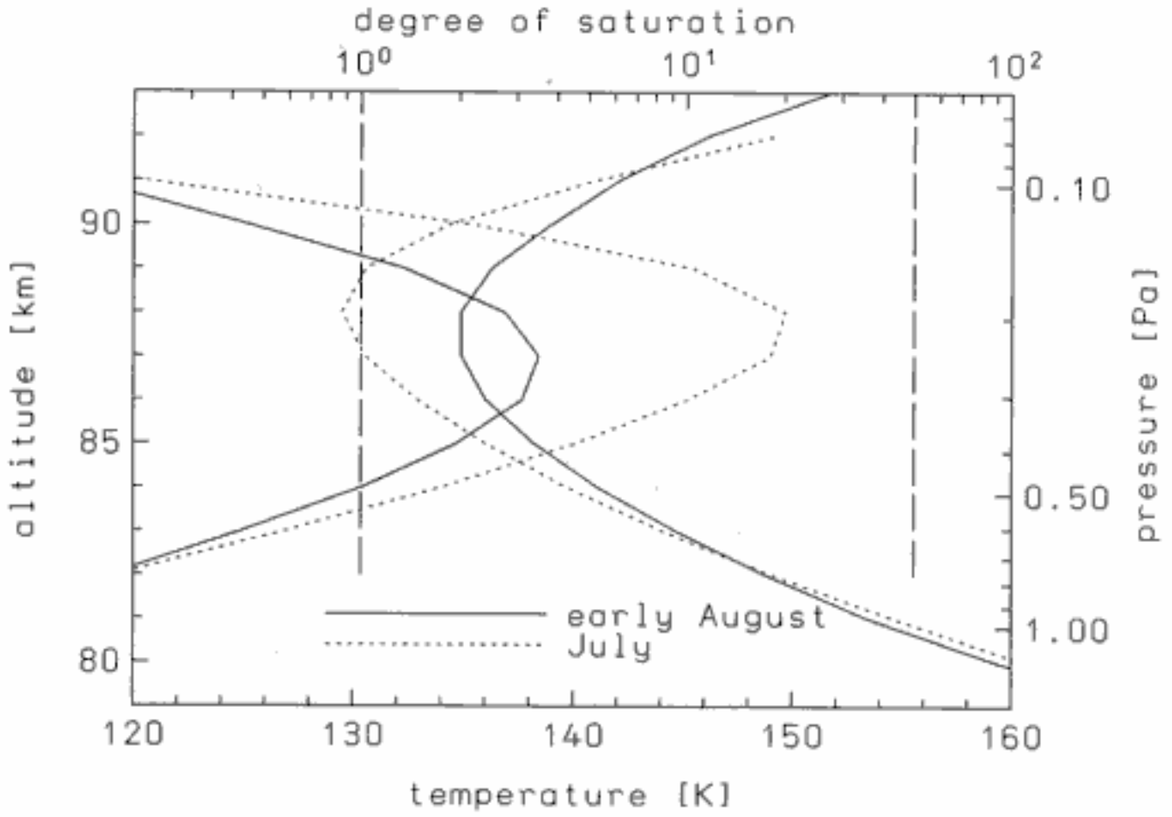

Figure 13. A section of the mean temperature profile from early August (solid line, this paper) and from July (dotted line, *Lübken and von Zahn* [1991]). We also show the corresponding profiles for the degree of saturation (top abscissa), assuming a water vapor mixing ratio of 1 ppmv. The dashed lines mark the critical values for supersaturation ($S = 1$) and for the degree of saturation required to initiate nonhomogeneous nucleation.

the summers of 1993 and 1994. A review of all measurements available shows that the mean summer temperature at the lower edge of NLC altitudes (82 km) is remarkably stable within the last 30 years; it was again and again observed to be in the range 150 ± 2 K (the variability at this altitude is only a few degrees within the summer season). This "equithermal submesopause" in summer puts a strong constraint on any model prediction of secular changes of mesospheric temperatures and related increasing occurrence rates for NLCs.

The mean altitude of the NLCs as determined from our lidar measurements is 83 km ± 1 km, which is very close to the very first height observations more than 100 years ago. We therefore conclude with a quotation from *Jesse's* [1896, p.161] original work, "... daß diese Höhe seit dem Beginn des Phänomens im Jahre 1885 stets nahe eine und dieselbe gewesen ist" (translated, "... that this altitude is one and the same since the beginning of this phenomenon in the year 1885"). It is conceivable that this repeatability in altitude reflects the repeatability in the thermal structure below the summer mesopause. The temperature in the NLC layer is persistently lower than 154 K. The NLCs are always observed below the mesopause. There is no apparent correlation between the conditions at the mesopause and the occurrence of NLCs at lower altitudes. The reason for this is presumably the fact that at our observation site there is a change of wind direction near 87 km altitude, which implies that the air mass at the mesopause stems from a different geographic location than the air at NLC heights.

Our results imply that nonstationarity and inhomogeneity in the horizontal structure are important factors when studying NLCs. We deduce this statement from our observation that the temperature and saturation conditions during our measurements are not closely related to the occurrence of NLCs. Lidar observations give the unique chance to observe the NLC layer as a function of time, thus gaining an insight into the temporal or the horizontal variability of the layer. Measuring the NLC layer by a rocket instrument and determining the thermal structure at a significant earlier or later point of time may give misleading results since the conditions may have changed between the various measurements.

The seasonal distribution of NLC and PMC observations at high latitudes reflects the thermal structure observed by in situ techniques. The sudden onset in mid-May and the sudden termination in mid-August are caused by a rather sudden change from winter to summer conditions and vice versa, respectively.

We conclude that observations of noctilucent clouds from the ground by lidar and by other means can be an important tool for gaining insight into the atmospheric background conditions near the Arctic mesopause. However, in order to understand details of the physical and chemical processes involved (including their relationship to the atmospheric environment), it is equally important to apply in situ techniques in the mesosphere and lower thermosphere.

Acknowledgments. We are grateful to Georg Witt, Tom Blix, and Frank Schmidlin for providing unpublished data from the NLC 1993 campaign. We thank Götz von Cossart for the information concerning NLC during the AEROSOL 2 campaign. Fruitful discussions with Ulf von Zahn have stimulated this work. We thank Rolf Becker for evaluating the falling sphere flights. We gratefully acknowledge the excellent support of the falling sphere flights by the crew of the Mobile Raketenbasis (Germany), and the Andøya Rocket Range (Norway). The rocket flights and the lidar operations were supported by the Bundesministerium für Bildung, Wissenschaft, Forschung und Technologie under grants No. 50 OE 9201 and 50 EE 94010.

References

Avaste, O., Noctilucent clouds, *J. Atmos. Terr. Phys.*, *55*, 133–143, 1993.

Balsiger, F., E. Kopp, M. Friedrich, K. M. Torkar, and U. Wälchli, Small-scale structure of O_2^+ and proton hydrates in a noctilucent cloud and polar mesospheric summer echo of August 9/10 1991 above Kiruna, *Geophys. Res. Lett.*, *20*, 2315–2318, 1993.

Balsiger, F., E. Kopp, M. Friedrich, K. M. Torkar, U. Wälchli, and G. Witt, Positive ion depletion in a noctilucent cloud, *Geophys. Res. Lett.*, *23*, 93–96, 1996.

Björn, L. G., E. Kopp, U. Hartmann, P. Eberhardt, P. H. G. Dickinson, D. J. Mackinnon, F. Arnold, G. Witt, A. Lundin, and D. B. Jenkins, Heavy ionospheric ions in the formation process of noctilucent clouds, *J. Geophys. Res.*, *90*, 7985–7998, 1985.

Cho, J., W. Swartz, M. Kelley, and C. Miller, CUPRI observations of PMSE during salvo B of NLC-91: Evidence of both partial reflection and turbulent scatter, *Geophys. Res. Lett.*, *20*, 2291–2294, 1993.

Cho, J. Y. N., and M. C. Kelley, Polar mesosphere summer radar echoes: Observations and current theories, *Rev. Geophys.*, *31*, 243–265, 1993.

Clancy, R. T., and D. W. Rusch, Climatology and trends of mesospheric (58-90 km) temperatures based upon 1982-1986 SME limb scattering profiles, *J. Geophys. Res.*, *94*, 3377–3393, 1989.

Fleming, E. L., S. Chandra, J. J. Barnett, and M. Corney, Zonal mean temperature, pressure, zonal wind, and geopotential height as functions of latitude, *Adv. Space Res.*, *10*(12), 11–59, 1990.

Fogle, B., and B. Haurwitz, Noctilucent clouds, *Space Sci. Rev.*, *6*, 279–340, 1966.

Forbes, J. M., Atmospheric tides, 2, The solar and lunar semidiurnal components, *J. Geophys. Res.*, *87*, 5241–5252, 1982.

Gadsden, M., The silver-blue cloudlets again: Nucleation and growth of ice in the mesosphere, *Planet. Space Sci.*, *29*, 1079–1087, 1981.

Gadsden, M., A secular change in noctilucent cloud occurrence, *J. Atmos. Terr. Phys.*, *52*, 247–251, 1990.

Gadsden, M., and W. Schröder, *Noctilucent Clouds*, Springer-Verlag, New York, 1989.

Garcia, R. R., Dynamics, radiation and photochemistry in the mesosphere: Implications for the formation of noctilucent clouds, *J. Geophys. Res.*, *94*, 14,605 – 14,615, 1989.

Giebeler, J., and F.-J. Lübken, Density and temperature measurements in the lower thermosphere with the CONE instrument, in *Proceedings of the 12th ESA Symposium on European Rocket and Balloon Programmes and Related Research, Lillehammer, Norway, Europ. Space Agency Spec. Publ., ESA SP–370*, 101–106, 1995.

Goldberg, R., E. Kopp, G. Witt, and W. Swartz, An overview of NLC-91: A rocket/radar study of the polar summer mesosphere, *Geophys. Res. Lett.*, *20*, 2443–2446, 1993.

Hansen, G., and U. von Zahn, Simultaneous observations of noctilucent clouds and mesopause temperatures by lidar, *J. Geophys. Res.*, *99*, 18,989–18,999, 1994.

Hansen, G., M. Serwazi, and U. von Zahn, First detection of a noctilucent cloud by lidar, *Geophys. Res. Lett.*, *16*, 1445–1448, 1989.

Hauchecorne, A., M.-L. Chanin, and P. Keckhut, Climatology and trends of the middle atmospheric temperature (33-87 km) as seen by Rayleigh lidar over the south of France, *J. Geophys. Res.*, *96*, 565–568, 1991.

Hillert, W., F.-J. Lübken, and G. Lehmacher, TOTAL: a rocket-borne instrument for high resolution measurements of neutral air turbulence during DYANA, *J. Atmos. Terr. Phys.*, *13/14*, 1835–1852, 1994.

Jensen, E., and G. E. Thomas, A growth-sedimentation model of polar mesospheric clouds: Comparisons with SME measurements, *J. Geophys. Res.*, *93*, 2461–2473, 1988.

Jesse, O., Untersuchungen über die sogenannten leuchtenden Wolken, *Meteorol. Z.*, *8*, 306–308, 1891.

Jesse, O., Die Höhe der leuchtenden Nachtwolken, *Astron. Nachr.*, *140*, 161–168, 1896.

Jones, J., and J. W. Peterson, Falling sphere measurements, 30 to 120 km, *Meteorol. Monogr.*, *8*, 176–177, 1968.

Kopp, E., F. Bertin, L. G. Björn, P. Dickinson, C. R. Philbrick, and G. Witt, The CAMP campaign 1982, in *Proceedings of the 7th ESA Symposium on European Rocket and Balloon Programmes and Related Research, Loen, Norway, Europ. Space Agency Spec. Publ., ESA SP–229*, 117–124, 1985.

Langer, M., K. Müller, and K. H. Fricke, Rayleigh lidar detection of aerosol echoes from noctilucent cloud altitudes at the Arctic Circle, *Geophys. Res. Lett.*, *22*, 381–384, 1995a.

Langer, M., K. P. Müller, K. H. Fricke, K. Römke, and F.-J. Lübken, Application of the Rayleigh-lidar technique to observations of noctilucent clouds, in *Proceedings of the 12th ESA Symposium on European Rocket and Balloon Programmes and Related Research, Lillehammer, Norway, Europ. Space Agency Spec. Publ., ESA SP–370*, 81–85, 1995b.

Lübken, F.-J., Aerodynamical effects in number density measurements in the lower thermosphere with the CONE instrument, *Adv. Space Res., (in press)*, 1996.

Lübken, F.-J., and U. von Zahn, Thermal structure of the mesopause region at polar latitudes, *J. Geophys. Res.*, *96*, 20,841–20,857, 1991.

Lübken, F.-J., et al., Mean state densities, temperatures and winds during the MAC/SINE and MAC/EPSILON campaigns, *J. Atmos. Terr. Phys.*, *52*, 955–970, 1990.

Lübken, F.-J., W. Hillert, G. Lehmacher, U. von Zahn, M. Bittner, D. Offermann, F. Schmidlin, A. Hauchecorne, M. Mourier, and P. Czechowsky, Intercomparison of density and temperature profiles obtained by lidar, ionization gauges, falling spheres, datasondes and radiosondes during the DYANA campaign, *J. Atmos. Terr. Phys.*, *13/14*, 1969–1984, 1994.

Marti, J., and K. Mauersberger, A survey and new measurements of ice vapour pressure at temperatures between 170 and 250 K, *Geophys. Res. Lett.*, *20*, 363–366, 1993.

Offermann, D., The DYANA campaign: A survey, *J. Atmos. Terr. Phys.*, *13/14*, 1639–1658, 1994.

Offermann, D., and H. H. Graef, Messungen der OH*-Temperatur, *Prometheus*, *2–4*, 125–128, 1992.

Olivero, J. J., and R. M. Bevilacqua, Physical properties affecting the existence of small ice particles in the mesosphere, *Space Res.*, *19*, 165–168, 1979.

Philbrick, C.R., J. Barnett, R. Gerndt, D. Offermann, W. P. Pendleton Jr, P. Schlyter, J. Schmidlin, and G. Witt, Temperature measurements during the CAMP program, *Adv. Space Res.*, *4*(4), 153–156, 1984.

Reid, G. C., Ice clouds at the summer polar mesopause, *J. Atmos. Sci.*, *32*, 523–535, 1975.

Russel, J. M., III, An interim reference model for the middle atmosphere water vapour distribution, *Adv. Space Res.*, *7*(9), 5–18, 1987.

Schmidlin, F. J., The inflatable sphere: A technique for the accurate measurement of middle atmosphere temperatures, *J. Geophys. Res.*, *96*, 22,673–22,682, 1991.

Schmidlin, F. J., First observation of mesopause temperatures lower than 100 K, *Geophys. Res. Lett.*, *19*, 1643–1646, 1992.

Smith, A. K., and G. P. Brasseur, Numerical simulation of the seasonal variation of mesospheric water vapour, *J. Geophys. Res.*, *96*, 7553–7563, 1991.

Taubenheim, J., G. von Cossart, and G. Entzian, Evidence of CO_2-induced progressive cooling of the middle atmosphere derived from radio observations, *Adv. Space Res.*, *10*(10), 171–174, 1990.

Taylor, M. J., and M. A. Hapgood, The effect of atmospheric screening on the visible border of noctilucent clouds, *J. Atmos. Terr. Phys.*, *46*, 363–372, 1984.

Thayer, J. P., N. Nielsen, and J. Jacobsen, Noctilucent cloud observations over Greenland by a Rayleigh lidar, *Geophys. Res. Lett.*, *22*, 2961–2964, 1995.

Theon, J.S., W. Nordberg, L. Katchen, and J. Horvath, Some observations on the thermal behavior of the mesosphere, *J. Atmos. Sci.*, *24*, 428–438, 1967.

Thomas, G.E., Solar Mesosphere Explorer measurements of polar mesospheric clouds noctilucent clouds, *J. Atmos. Terr. Phys.*, *46*, 819–824, 1984.

Thomas, G. E., Mesospheric clouds and the physics of the mesopause region, *Rev. Geophys*, *29*, 553–575, 1991.

Thomas, G. E., Climatology of polar mesospheric clouds: Interannual variability and implications for long-term trends, in *The Upper Mesosphere and Lower Thermosphere: A Review of Experiment and Theory, Geophys. Monogr. Ser.*, vol.87, edited by R. M. Johnson and T. L. Killeen, pp.185–200, AGU, Washington, D.C., 1995.

Thomas, G. E., and C. P. McKay, On the mean particle size and water content of the polar mesospheric clouds, *Planet. Space Sci.*, *33*, 1209–1224, 1985.

Thomas, G. E., J. J. Olivero, E. J. Jensen, W. Schröder, and O. B. Toon, Relation between increasing methane and the presence of ice clouds at the mesopause, *Nature*, *338*, 490–492, 1989.

Thomas, L., A. K. P. Marsh, D. P. Wareing, and M. A. Hassan, Lidar observations of ice crystals associated with noctilucent clouds at middle latitudes, *Geophys. Res. Lett.*, *21*, 385–388, 1994.

Turco, R. P., O. B. Toon, R. C. Whitten, R. G. Keesee, and D. Hollenbach, Noctilucent clouds: Simulation studies of their genesis, properties and global influences, *Planet. Space Sci.*, *3*, 1147–1181, 1982.

von Zahn, U., E. V. Thrane, and R. Skatteboe, The ALOMAR project: Status and outlook, in *Proceedings of the 12th ESA Symposium on European Rocket and Balloon Programmes and Related Research, Lillehammer, Norway, Europ. Space Agency Spec. Publ., ESA SP–370*, 379–386, 1995.

Wilhelm, N., and G. Witt, The SLIPS, a Scattered Light Intensity Profile Sensor for rocket-borne investigations of

noctilucent clouds, in *Collection of Works of the International Workshop on Noctilucent Clouds*, pp.69–80, Valgus, Tallinn, Estonia, 1989.

Witt, G., Height, structure, and displacements of noctilucent clouds, *Tellus 14*(1), 1–18, 1962.

Witt, G., Optical characteristics of mesospheric aerosol distributions in relation to noctilucent clouds, *Tellus 20*(1), 99–113, 1968.

Zadorozhny, A. M., A. A. Tyutin, G. Witt, N. Wilhelm, U. Wälchli, J. Cho, and W. E. Swartz, Electric field measurements in the vicinity of noctilucent clouds and PMSE, *Geophys. Res. Lett.*, *20*, 2299–2302, 1993.

K.-H. Fricke, M. Langer, and F.-J. Lübken, Physikalisches Institut der Universität Bonn, Nussallee 12, 53115 Bonn, Germany. (email: luebken@pib1.physik.uni-bonn.de)

(Received October 16, 1995; revised January 22, 1996; accepted January 23, 1996.)